Fall 2017

Thermal Performance of a Double-Pipe Heat Exchanger with a Koch Snowflake Fractal Design

Anton Gomez

THERMAL PERFORMANCE OF A DOUBLE-PIPE HEAT EXCHANGER WITH A KOCH SNOWFLAKE FRACTAL DESIGN

by

ANTON GOMEZ

(Under the Direction of David Calamas)

ABSTRACT

Double-pipe heat exchangers are the simplest type of heat exchanger and are widely utilized in industrial applications. The effectiveness of double-pipe heat exchangers can be increased by using various heat transfer enhancement techniques. Passive heat transfer enhancement methods are desirable as they do not require moving components and are easy to manufacture and maintain. The focus of this study is to implement a passive heat transfer enhancement method and to investigate how thermal performance is impacted. Specifically, the inner pipe in a heat exchanger will be modified to have a cross-section in accordance with the Koch snowflake fractal pattern. The Koch snowflake fractal pattern, when utilized in the heat exchanger, results in an increase in surface area. A validated and verified model of a double-pipe heat exchanger will be used to evaluate the effectiveness of double-pipe heat exchangers inspired by the first three iterations of the Koch snowflake fractal pattern. The performance of the fractal heat exchangers will be compared to a traditional double-pipe heat exchanger operating under identical conditions. It was found that a double-pipe heat exchanger with a cross-section in accordance with the second iteration of the Koch snowflake fractal pattern resulted in an increase in the overall heat transfer coefficient and heat transfer rate of 18% and 75% respectively when compared with a traditional double-pipe heat exchanger with a circular cross-section.

INDEX WORDS: Thesis, Koch snowflake, Double-pipe heat exchanger, Fractal geometry, Surface enhancement, College of Graduate Studies, Georgia Southern University

THERMAL PERFORMANCE OF A DOUBLE-PIPE HEAT EXCHANGER WITH A KOCH SNOWFLAKE FRACTAL DESIGN

by

ANTON GOMEZ

B.S., Georgia Southern University, 2015

A Thesis Submitted to the Graduate Faculty of Georgia Southern University in

Partial Fulfillment of the Requirements for the Degree

MASTER OF SCIENCE

STATESBORO, GEORGIA

THERMAL PERFORMANCE OF A DOUBLE-PIPE HEAT EXCHANGER WITH A KOCH SNOWFLAKE FRACTAL DESIGN

by

ANTON GOMEZ

Major Professor:	David Calamas
Committee:	Mosfequr Rahman
	Marcel Ilie

Electronic Version Approved:

December 2017

DEDICATION

To my family and friends for their support.

ACKNOWLEDGMENTS

I would like to acknowledge Dr. David Calamas for his guidance as my advisor and for providing the research opportunity in this topic.

TABLE OF CONTENTS

Page

LIST OF TABLES

LIST OF FIGURES

INTRODUCTION

Background

Double-Pipe Heat Exchanger

Double-pipe heat exchangers (DPHE) are devices that exchange heat between two fluids of different temperatures that are separated by a solid wall. They are utilized in a wide variety of applications including refrigeration, air conditioning, power plants, and petroleum refineries, among others. The DPHE is one of the simplest types of heat exchangers and consists of two concentric pipes of different diameters. One fluid in a double-pipe heat exchanger flows through the smaller inside pipe while the second fluid flows through the annular space between the two pipes.

The flow in a DPHE can be classified into two flow configurations: co-current (parallel flow) or counter-current (counter flow) as exhibited in Fig. 1. In parallel flow, the hot and cold fluid enter the double-pipe heat exchanger on the same side and move in the same direction. In counter flow, the hot and cold fluids enter on opposite sides and flow in opposite directions. In a counter flow heat exchanger the outlet temperature of the cold fluid may exceed the outlet temperature of the hot fluid. However, the outlet temperature of the cold fluid cannot surpass the inlet temperature of the hot fluid. The rate of heat transfer in a double-pipe heat exchanger is directly proportional to the log mean temperature difference. Assuming identical operating conditions, a counter flow heat exchanger always has a greater log mean temperature difference then a parallel flow heat exchanger and is thus more effective.

In a double-pipe heat exchanger, heat is transferred from the hot fluid to the wall separating the two concentric pipes by conduction. Then, heat is transferred through the wall by convection.

Finally, heat is transferred from the wall to the second fluid in the annular space by convection. It is desirable to use an inner pipe of a small diameter and made of a material with a high conductivity to minimize the conduction resistance between the two fluids. In addition, it is often assumed that the outer surface of the heat exchanger is perfectly insulated, or adiabatic (i.e. no heat is lost to the surroundings). Finally, heat exchangers can be assumed to be steady-flow devices as they typically operate for long durations of time without changes in their operating conditions.

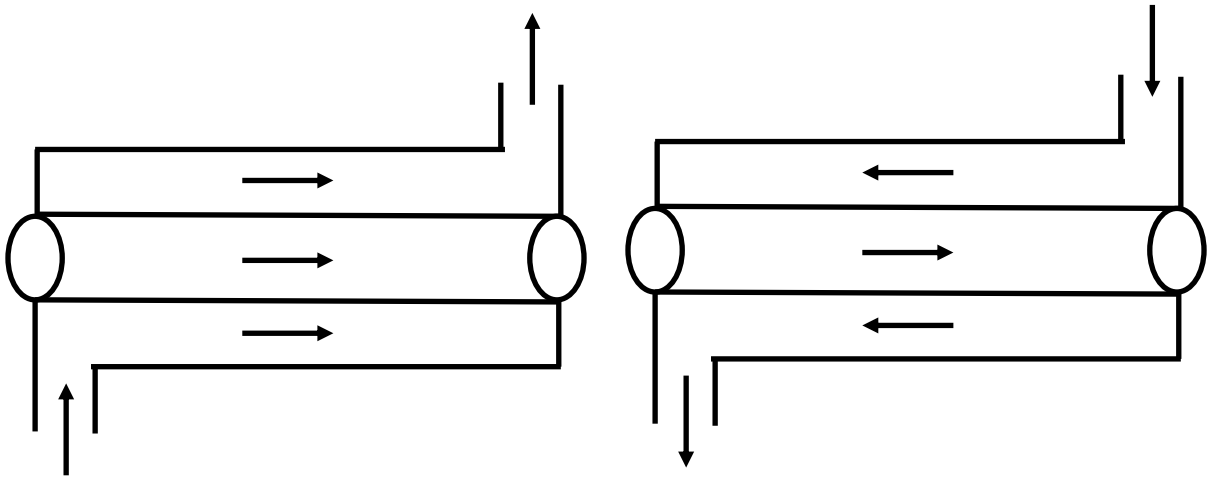

Figure 1 Parallel Flow (left) and Counter Flow (right). [1]

Due to the simplicity and wide usage of double-pipe heat exchangers in industrial applications, it is highly desirable to improve their effectiveness. This is often done through various heat transfer enhancement techniques. For example, artificially roughening the surface of the pipes (or utilizing fins) can drastically increase the heat transfer rate when the flow is turbulent. Unfortunately, an increase in surface roughness results in an increase in pressure drop and thus pumping power. Bergles denoted that the study of heat transfer improvement is usually represented as heat transfer enhancement, intensification, or augmentation. In general, that means an increase in the heat transfer coefficient [2].

Heat transfer enhancement methods fall into three main categories: active methods, passive methods, and compound methods. Mohamad et al. developed a comprehensive review of DPHE that discussed, in detail, the aforementioned methods used for heat transfer enhancement [3]. The authors explained that active methods involve the use of an external force to increase heat transfer. Some examples include: reciprocating plungers, implementing a magnetic field for flow disturbance, using surface or flow vibration, and applying electromagnetic fields. In passive methods, no external forces are used for heat transfer enhancement. Instead, surface or geometric alterations are utilized to enhance the rate of heat transfer. Modifications, such as twisted tape inserts or fins are very common due to their simplicity, low cost and easy installation and maintenance. Surface modifications enhance the heat transfer coefficient and thus heat transfer rate but often result in an increase in pressure drop.

Another passive method of interest involves changes to the geometry of the pipe. This typically involves altering the cross-section of the heat exchanger. Maximizing the surface area of the wall between the two fluids improves the efficiency of the heat exchanger but as with surface treatments, often results in an increase in pressure drop. The compound method of heat transfer enhancement involves the combination of both passive and active methods, which makes it the least common of the three.

In this study, a passive method of heat transfer enhancement was investigated, by modifying the geometry of the inner pipe to increase the surface area of heat transfer. A traditional double-pipe heat exchanger consists of two concentric pipes with circular cross-sections. In this work, the inner pipe will be replaced with a pipe with a cross-section inspired by the Koch snowflake fractal pattern. The use of the Koch snowflake fractal pattern will result in an increase in surface area per unit volume of the heat exchanger.

Koch Snowflake Fractal

Fractals, are never ending patterns that can be found in nature. They are infinitely complex patterns that repeat a simple process for a finite number of iterations or ad infinitum. Fractal patterns may be familiar to most because they can be found in nature. Some examples are the vascular system in plants and animals, human lungs, trees, rivers, coastlines, mountains, clouds, seashells, snowflakes, among many other. Although they may be only perceived as an infinitely repeating pattern, fractals have been studied by mathematicians as early as the 17^{th} century for their unique characteristics. In the present, fractals have played an important role in research among scientists and engineers. Huang et al. presented some applications of the current use of fractals in heat transfer. [4].

A fractal pattern of interest is one that was first introduced by Swedish mathematician, Helge von Koch in 1904. The Koch snowflake is of interest because of its particular behavior. As the number of fractal iterations increases, so does the perimeter of the Koch snowflake, ad infinitum. However, while the perimeter could theoretically increase infinitely, the geometry is contained within a finite area which is dependent on the original size of the zeroth iteration. The Koch Snowflake is built by starting with an equilateral triangle (zeroth fractal iteration), removing the inner third of each side, building another equilateral triangle at the location where the side was removed, and then repeating the process indefinitely. Each repetition is denoted as a fractal iteration. For example, iteration zero is represented as $n = 0$, iteration one as $n = 1$, and so on. The zeroth and first three fractal iterations of the Koch Snowflake fractal are illustrated in Fig. 2. The number of sides for the zeroth iteration is that of an equilateral triangle. As the iteration increments Eq. (1) is used to determine the number of sides.

$$N = 3 * 4^n \tag{1}$$

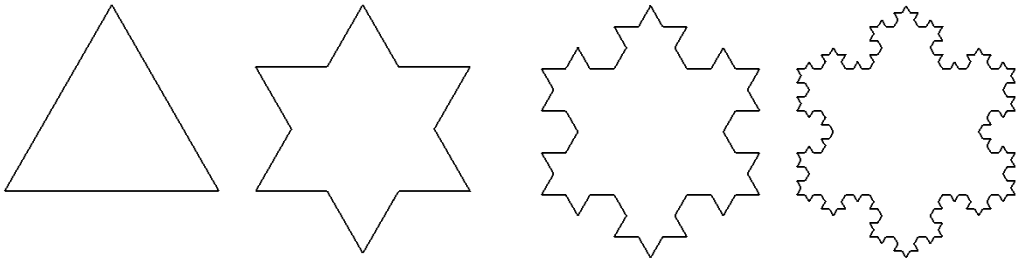

Figure 2 Koch Snowflake Fractal Iterations

The length of the side of the Koch Snowflake, denoted as *l*, can be calculated by using Eq. (2).

$$l = s * 3^{-n} \tag{2}$$

The perimeter of the Koch Snowflake is dependent on the level of fractal iteration, *n*, and the length of the side, *s*, of the initial equilateral triangle from iteration *n* = 0. The equation to calculate the perimeter is presented below in Eq. (3).

$$P = (3s)\left(\frac{4}{3}\right)^n \tag{3}$$

The area of the Koch Snowflake is only dependent on the length of the side, *s*, of the initial equilateral triangle of iteration *n* = 0, as seen in Eq. (4).

$$A_{n=0} = \frac{\sqrt{3}}{4}s^2 \tag{4}$$

For iteration *n* = 1 the area will be the area of the original equilateral triangle plus the area of three smaller equilateral triangles, as seen in in Eq. (5).

$$A_{n=1} = \frac{\sqrt{3}}{4}s^2 + 3\frac{\sqrt{3}}{4}\left(\frac{s}{3}\right)^2 \tag{5}$$

And so on, for iteration $n = 2$, as seen in Eq. (6) and for iteration $n = 3$, as seen in Eq. (7).

$$A_{n=2} = \frac{\sqrt{3}}{4}s^2 + 3\frac{\sqrt{3}}{4}\left(\frac{s}{3}\right)^2 + 3 * 4\frac{\sqrt{3}}{4}\left(\frac{s}{3^2}\right)^2 \tag{6}$$

$$A_{n=3} = \frac{\sqrt{3}}{4}s^2 + 3\frac{\sqrt{3}}{4}\left(\frac{s}{3}\right)^2 + 3 * 4\frac{\sqrt{3}}{4}\left(\frac{s}{3^2}\right)^2 + 3 * 4 * 4\frac{\sqrt{3}}{4}\left(\frac{s}{3^3}\right)^2 \tag{7}$$

Generating a summation of a geometric series, whenever *n* approaches infinity the equation for the area of the Koch Snowflake simplifies to Eq. (8).

$$A_{n\to\infty} = \frac{2\sqrt{3}}{5}s^2 \tag{8}$$

An increment in perimeter is observed as the Koch Snowflake fractal iteration is increased. For example, for an initial side length of $s = 18$ mm, a relationship between perimeter side length ratio and fractal iteration is observed in Fig. 3. It is observed that for every iteration there is a significant increase in the perimeter of the geometry. At the fourth fractal iteration, an increase of approximately 200% of the initial perimeter is experienced.

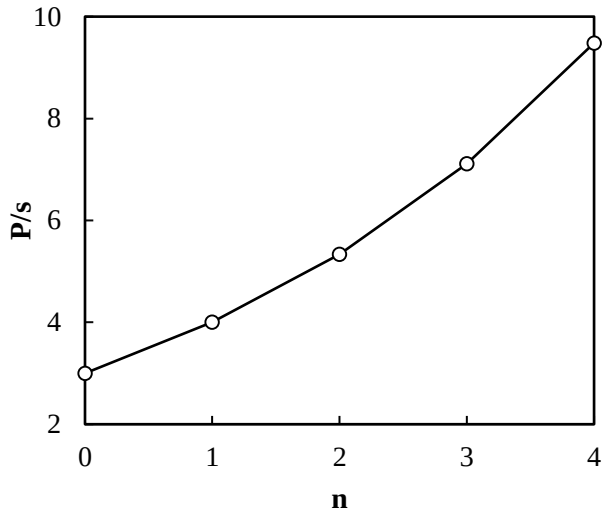

Figure 3 Perimeter Side Length Ratio and Fractal Iteration

The relationship of area of the Koch Snowflake and the increment in fractal iteration with same initial side length of s = 18 mm is illustrated in Fig. 4. The ratio of areas is the area of each iteration of Koch Snowflake over the area of Koch Snowflake when n approaches infinity. Unlike the significant increase of perimeter, the area, when compared for each iteration it is observed to be fundamentally nearly the same. This represents the behavior of the Koch Snowflake fractal. As the number of fractal iteration increases, the area of the geometry remains finite.

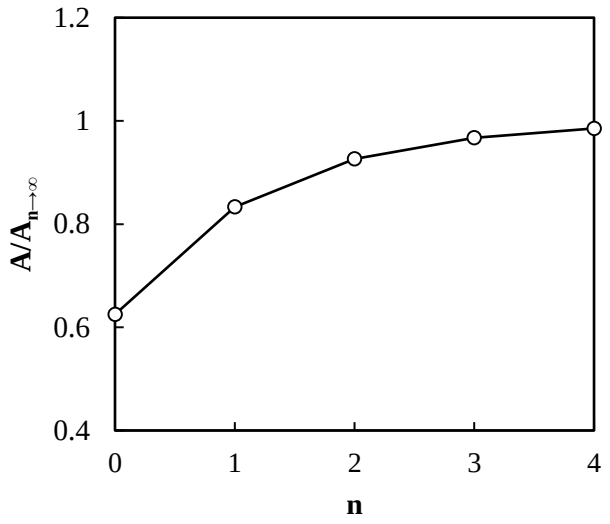

Figure 4 Area Ratio and Fractal Iteration

The Koch Snowflake fractal is special in its behavior. It allows an infinite increase in perimeter while preserving a finite area. If this concept is translated into a Koch Snowflake pipe geometry inside a DPHE, conceptually, an infinite surface area can be achieved while maintaining a finite cross sectional area. A numerical study using computational fluid dynamics of a modified pipe geometry is presented in this study, and compared to a traditional cylindrical pipe geometry.

Motivation

Heat exchangers are widely utilized in industry in a wide range of applications, from heating and air-conditioning to power production. The simplest type of heat exchanger, the double-pipe heat exchanger, has garnered very few effective heat transfer enhancements. Improving the effectiveness of such a commonly utilized heat exchanger is extremely desirable. As passive heat transfer enhanced methods require no moving mechanical components, they are extremely desirable. Unfortunately, experimentally examining various passive heat transfer enhancement methods is both time consuming and expensive due to manufacturing constraints. Fortunately, the advent of Computational Fluid Dynamics (CFD) has alleviated some of the need for experimental testing. In this study, the cross-sectional geometry of the inside pipe in a double-pipe heat exchanger will be modified in accordance with the Koch snowflake pattern. By modifying the cross-sectional geometry, a significant increase in the surface area available for convective heat transfer can be achieved without increasing the package volume of the heat exchanger.

Objectives

The objectives of this study is to: (1) create a computational model of a traditional double-pipe heat exchanger, (2) validate the physics of the model and verify a grid independent solution, (3) modify the inside pipe to incorporate a fractal cross-section in accordance with the Koch snowflake pattern, and (4) compare the performance of the fractal heat exchanger to that of a traditional heat exchanger with a circular cross-section.

Literature Review

In this section, the literature that has been conducted throughout the years to study the performance of DPHE using computational numerical simulations, is summarized. Numerical simulations have

been extensively used to analyze the performance of DPHE to calculate thermal and hydrodynamic characteristics. Computational fluid dynamics (CFD) is a tool that uses numerical analysis to solve problems that involve fluid flows. It has been widely used in the study of fluid flow and heat transfer, including heat exchangers. Several studies have carried experimental and CFD analysis on heat exchangers to validate the method.

Ibrahim examined important parameters that included heat transfer coefficient and friction factor, to be able to determine heat transfer rate and pressure drop. He compared the existing theoretical correlations found in literature, with the CFD, and experimental results. A two-dimensional, and a k-ε turbulent model were utilized in the numerical simulation setup to find the heat transfer coefficient. He concluded that the results obtained by CFD were in good agreement with both experimental data and empirical correlations. Revealing that CFD is an accurate tool to predict heat transfer coefficient in heat exchanger with turbulent flows [5].

Van der Vyer et al. provided a two-part investigation. First, a three-dimensional simulation of a DPHE compared CFD, empirical correlations, and experimental results. The simulation was performed using k-ε for a standard turbulent model. With the assumption of an adiabatic outer wall, which was not modelled, to help in the reduction of CPU time. The temperature and pressure at the inlets and outlets were determined so that heat transfer, Nusselt number, and friction factor could be calculated. When comparing between CFD results and experimental results the average error was found to be 5.5% with the correlation. It was concluded that the CFD results showed good agreement. Due to this, it is feasible to model a prototype configuration of a DPHE. The second part of her investigation, involved using CFD on a modified DPHE design. Although discussed later into more depth, her investigation, using CFD as a tool, helped in finding the

thermal and hydrodynamic characteristics before investing in manufacturing costs and time when developing a new heat exchanger design [6].

In a numerical investigation, Arslan studied a steady state turbulent forced flow on a DPHE with a horizontal smooth, semi-circle as the inner pipe. The investigation aimed to compare the Nusselt number and Darcy friction factor with a modified pipe geometry, but also compare the different available turbulence models (k-ε Standard, k-ε Realizable, k-ε RNG, k-ω Standard and k-ω SST) and their results. The results show that as the Reynolds number increased Nusselt number increased but Darcy friction factor decreased. As for the turbulent models, it was obtained that, k-ε Standard, k-ε Realizable, and k-ε RNG were the most suitable turbulence models for his investigation [7].

Kumar et al. presented a work that investigated the hydrodynamic and heat transfer characteristics of a DPHE. A numerical study of a counter-current configuration with hot fluid in the inner pipe side and cold fluid in the annulus area, was compared against experimental data. The overall heat transfer coefficients, Nusselt numbers, and friction factors from the inner and outer pipes were compared with experimental data collected, as well as reported in the literature. The CFD simulation results were found to be in good agreement with the experimental data, with Nusselt number values with 4% error for inner pipe and 10% error in the outer pipe. A reasonable comparison was found between the literature data and simulations [8].

Bhanuchandrarao et al. conducted a numerical analysis to compare the performance of a parallel and counter flow DPHE. Using the standard based k-ε turbulence model the analyses were conducted for three different velocities and seven different fluids. The results of the thermal performance obtained from the simulations were compared with theoretical correlations. It was

concluded that the CFD results were found to be consistent with theoretical calculations with most valued within 5% of each other [9].

Studies, which have modified the pipe geometry, to maximize surface area, and therefore increase heat transfer rate, are discussed in detail in the following paragraphs. Chen and Dung studied the temperature, pressure, and velocity contours. They calculated the Nusselt number and overall heat transfer coefficient on parallel-flow and counter-flow DPHE with inner pipes of alternating, horizontal and vertical, oval cross-section pipes. The computational model was simulated using only laminar flow with a maximum Reynolds number of 2000, and compared to a DPHE with circular pipes. The results showed that the modification of the pipe's cross-section geometry improved the heat transfer performance, in this case with a parallel flow arrangement [10].

Bhadouriya et al. performed three-dimensional numerical simulations for laminar and turbulent flow regimes to analyze enhancement in heat transfer and pressure drop of air flow inside a twisted square duct. In their paper the validation of the experimental setup consisted on simulations over a straight square duct geometry. When comparing the straight square duct against a twisted square duct geometry, while considering constant pumping criteria, it was concluded that twisted square duct is more advantageous in laminar flow conditions with an enhancing factor of 10.5 [11].

Meyer and Van der Vyver work is of importance due to the implementation of a fractal pattern on a DPHE. A quadratic Koch island fractal pipe design was investigated using three techniques: by analytical, numerical, and experimental methods. The pipe inspired from fractals increases the pipe's surface area thus increasing the heat transfer area significantly. As the fractal iterations increased, heat transfer rate increased. The model targeted the comparison of heat transfer and pumping power amongst different iterations of fractal pipe geometries. The k-ε model for standard turbulent flow was used for the simulations. A range of Reynolds numbers of 4500 to 90000 were

studied for the pipe, and 3500 to 50000 for the shell. The analytical model was found to be in good agreement with the numerical predictions in a way that heat transfer increased by a factor of two for each iteration. The experimental results also confirmed that the numerical simulation results closely matched the heat transfer increase found [12].

Wang et al. presented a numerical study of turbulent flow and heat transfer of air in a set of regular polygonal (non-circular) ducts and circular pipe. The k-ε turbulence model was used for ducts with the same hydraulic diameter as their characteristics lengths in the Reynolds number. The polygonal geometries simulated included: equilateral triangle, square, regular hexagonal, regular octagonal, and regular dodecagonal. It was concluded that for a cylindrical pipe, the numerical results agree well with the experimental correlations. And for the polygonal ducts, the heat transfer coefficient in the duct corner region is lower than any other part of the wall pipe. The smaller the angle of the corner region, the more it deteriorated the circumferential local heat transfer coefficient becomes [13].

Another technique to enhance the thermal performance of a DPHE is the addition of fins to the pipe to increase surface area, or the addition of inserts to alter the flow behavior. Kumar et al. investigated the performance of three different DPHE with rectangular, triangular, and parabolic fin profiles. Numerical analysis was conducted at a various mass flow conditions. A parallel flow configuration and Reynolds numbers between 100 and 1000. The results suggested a heat transfer enhancement in the finned pipe compared against the un-finned one [14].

Hameed and Essa provided research of an experimental and numerical investigation to evaluate the performance of a triangular finned DPHE. The experimental section was conducted on a smooth and finned pipe heat exchanger. The experimental results showed an enhancement in heat dissipation for triangular pipes of 3 to 4 times more than the traditional smooth pipe. When

comparing with the numerical results, which showed good agreement with a 4% difference between experimental and numerical results, it was concluded an augmentation in heat transfer in the triangular finned pipe due to the increase in surface area [15].

Verma and Kumar performed an analysis on a double pipe heat exchanger with helical tap inserts at the annulus of the inner pipe. With the idea to enhance the thermal characteristics of the heat exchanger. The Nusselt number and friction factor were obtained from a three-dimensional simulation using the SST k-ω turbulent model. The results found, were that helical tape inserts in the annulus increase velocity and surface area enabling the enhancement of heat transfer but also an increase of pressure drop is observed [16].

In an innovative design, Hashenheim et al. studied a DPHE with conical pipes. The modified geometry improved thermal performance while reducing the weight of the device. The simulations were performed for Reynolds number from 12000 to 50000 using the k-ε turbulence model. Parameters, such as the Nusselt number and friction factor were numerically investigated. It was concluded that the modified conical geometry of the DPHE produced an increase in heat transfer rate of 54% and Nusselt number incremented by 63% [17].

A summary of the aforementioned literature indicates that an increase in heat transfer can achieved through modifications to the surface of the heat exchanger. What has received little attention is the use of fractal geometries in the design of heat exchangers. In this study, the Koch snowflake pattern will be utilized to increase the convective surface area of a double-pipe heat exchanger without changing the package volume. The performance of this fractal heat exchanger will be compared with that of a traditional double-pipe heat exchanger.

CHAPTER 1: HEAT TRANSFER IN A FRACTAL DPHE

Introduction

Passive methods for heat transfer enhancement techniques are common in a DPHE. When analyzing the performance of double-pipe heat exchangers it is important to note the difference between thermal performance and hydraulic performance. If the goal is to minimize pressure drop, and thus pumping power, modifications to the surface are sometimes undesirable. However, if the goal is to increase the surface area to volume ratio of the heat exchanger than surface modifications are often advantageous. This work will focus on heat transfer enhancement rather than pumping power minimization. In this study, heat transfer enhancement will be achieved by modifying the cross-sectional geometry of the inside pipe in a double-pipe heat exchanger in accordance with the Koch snowflake fractal pattern. The increase in surface area that can be achieved with the Koch snowflake design is highly dependent upon the fractal iteration. Therefore, double-pipe heat exchangers with cross-sections in accordance with the first three fractal iterations of the Koch snowflake fractal pattern will be investigated.

Heat Transfer Analysis on Koch Snowflake DPHE

Heat transfer inside a DPHE consists of exchange of thermal energy between a cold fluid and a hot fluid with a solid wall (pipe) separating both. Three heat transfer operations occur: convective heat transfer from the inner fluid to the inner wall of the pipe, conductive heat transfer through the pipe wall, and convective heat transfer from the outer pipe wall to the outside fluid. In this section, some theoretical correlations for the heat transfer analysis of a DPHE are introduced. The heat transfer rate, overall heat transfer coefficient, and effectiveness are explained in this section for

further understanding of the heat transfer enhancement of the Koch Snowflake DPHE. To find the rate of heat transfer between the two fluids the following equation Eq. (9) is applied

$$\dot{Q} = \frac{\Delta T}{R} = U A_s \Delta T_{lm} \tag{9}$$

where R is the total thermal resistance that associates both convection and conduction as seen in Eq. (10), ΔT is the log mean temperature difference, A_s the surface area of the wall, and U is the overall heat transfer coefficient expressed in Eq. (11),

$$R = \frac{1}{h_i A_i} + \frac{\log \frac{D_o}{D_i}}{2\pi k L} + \frac{1}{h_o A_o} \tag{10}$$

$$U = \frac{1}{R A_s} \tag{11}$$

where h_i and h_o are the heat transfer coefficients of the fluids and k is the thermal conductivity of the wall, D_i and D_o, inner and outer hydraulic diameters, respectively. And, A_i and A_o the inner surface of the wall and outer surface of the wall separating the two fluids, respectively. The heat transfer coefficient for either cold or hot fluids is expressed as in Eq. (12),

$$h = \frac{kNu}{D_h} \tag{12}$$

where k is the thermal conductivity of the cold or hot fluid, D_h the hydraulic diameter and Nu the Nusselt number found by using the Gnielinski correlation for turbulent flows as in Eq. (13),

$$Nu = \frac{\left(\frac{f}{8}\right)(Re - 1000)Pr}{1 + 12.7\left(\frac{f}{8}\right)^{\frac{1}{2}}\left(Pr^{\frac{2}{3}} - 1\right)} \tag{13}$$

where Pr is the Prandtl number, Re the Reynolds number, and f is the friction factor later described in Chapter 2.

In order to increase the rate of heat transfer in a double-pipe heat exchanger the overall heat transfer coefficient must be increased. Alternatively, the surface area of the heat exchanger could be increased. It should be noted that the surface area of the heat exchanger should be increased without increasing the package volume of the heat exchanger. This can be accomplished with the Koch snowflake fractal pattern. By increasing the surface area of the heat exchanger through the use of the Koch snowflake fractal pattern, an increase in the total heat transfer rate should be achieved.

It should be noted that the log mean temperature difference method used in the analysis of heat exchangers is used to determine the size of a heat exchanger to achieve prescribed outlet temperatures when the operating conditions are known. In this analysis, the size of the heat exchanger is known because the size of the pipes are already defined by the Koch snowflake fractal pattern. Thus, the log mean temperature difference method is not suitable for this analysis. In this analysis, the rate of heat transfer and fluid outlet temperatures should be determined in order to characterize the performance. Again, in this case, the operating conditions (flow rates and inlet temperatures) and size of the heat exchanger are known. The goal of this study is to determine the heat transfer performance of double-pipe heat exchangers inspired by the Koch snowflake fractal pattern. Therefore, the effectiveness-NTU method will be employed rather than the log mean temperature difference method. The effectiveness of the heat exchanger is the ratio of the actual heat transfer rate to the maximum possible heat transfer rate. NTU stands for the Number of Transfer Units and it is largely a measure of the size, or heat transfer area, of the heat exchanger.

If the effectiveness, ε, is obtained through equation Eq. (14), specifically for counter flow configurations, then it is possible to calculate the rate of heat transfer.

$$\varepsilon = \frac{1 - \mathrm{e}^{(-\mathrm{NTU}(1-\mathrm{c}))}}{1 - \left(ce^{(-NTU(1-c))}\right)} \tag{14}$$

where *c*, is the heat capacity ratio as seen in equation Eq. (15) and *NTU* is the number of transfer units obtained by equation Eq. (16) as follows

$$c = \frac{C_{min}}{C_{max}} \tag{15}$$

$$NTU = \frac{UA_s}{C_{min}} \tag{16}$$

where C_{min} is the smaller heat capacity rate which will experience a larger temperature change. Using this concept, it is possible to obtain the maximum heat transfer rate as in Eq. (17), and consequently the actual rate of heat transfer using equation Eq. (18).

$$\dot{Q}_{max} = C_{min}\left(T_{h,in} - T_{c,in}\right) \tag{17}$$

$$\dot{Q} = \varepsilon \dot{Q}_{max} \tag{18}$$

CHAPTER 2: COMPUTATIONAL FLUID DYNAMICS

Introduction

In this section, a computational fluid dynamics model of a traditional double-pipe heat exchanger and several fractal double-pipe heat exchangers will be developed. The computational model's physics will be validated with known theoretical solutions. In addition, the computational models will be verified for grid independent solutions. After validating and verifying the computational models, the performance of a double-pipe heat exchanger with a fractal cross-section will be compared with that of a traditional double-pipe heat exchanger with a circular cross-section.

Koch Snowflake DPHE

A three-dimensional DPHE with a modified Koch Snowflake fractal inner pipe was modeled using SolidWorks, a commercially available CAD software. Four different models were generated, one for each of the first three fractal iterations, and one for a traditional circular cross section pipe geometry for comparison and validation purposes. The dimensions of the traditional DPHE are shown in Table 1.

Table 1 Dimensions of Double Pipe Heat Exchanger

DPHE Dimensions (mm)	
Inner Pipe Diameter	15
Inner Pipe Thickness	2
Outer Pipe Diameter	32
Pipe Length	1000

A zoom-in of the solid geometry of the inner fluid, inner cylindrical pipe, and outer fluid of the DPHE with the dimensions of Table 1 is shown in Fig. 5. The origin and axis of reference for XY

and YZ are illustrated in Fig. 6. These reference axes are of relevance to understand the orientation of the thermal contours obtained and exhibited further into the study. The outer pipe of the DPHE was not modeled, but it was still taken into consideration. In other words, it was assumed that the outer surface of the heat exchanger was perfectly insulated, or adiabatic.

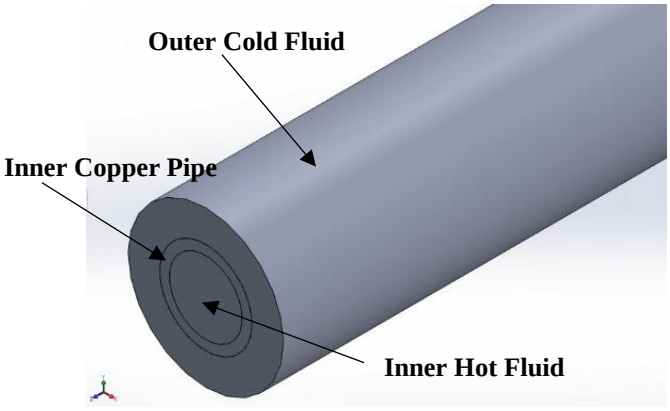

Figure 5 Close-Up View of DPHE Solid Model

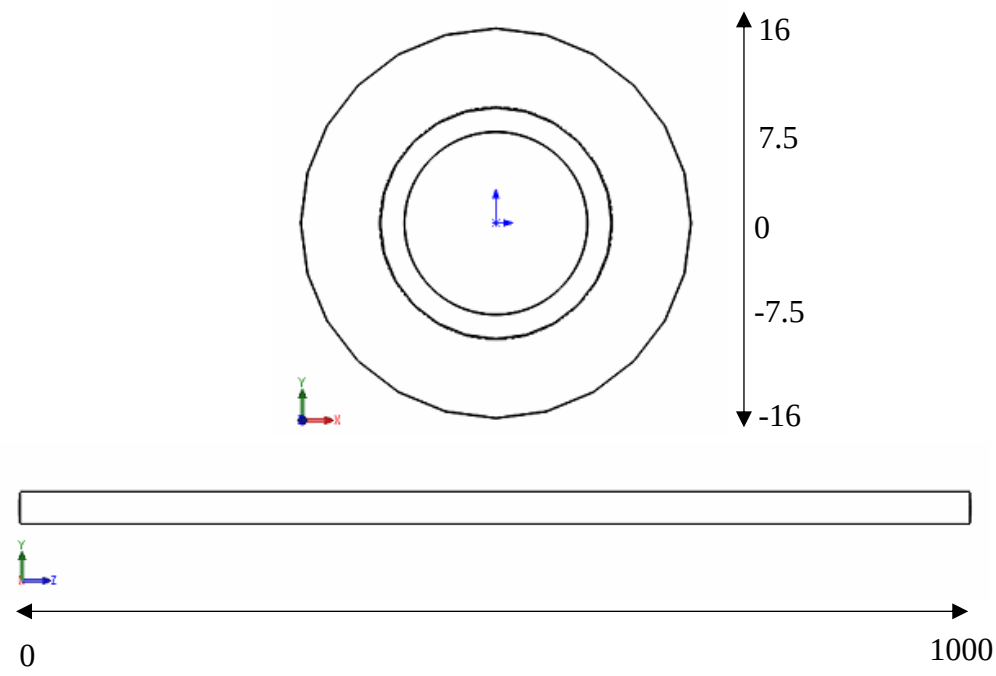

Figure 6 Origin and Axis of Reference of DPHE in Millimeters

The modified Koch Snowflake pipes for iteration $n = 0$, $n = 1$, and $n = 2$ were also modeled using SolidWorks. The pipe thickness was representative of a traditional pipe thickness, based on the wall schedule, for the pipe hydraulic diameter used in this analysis. The three different pipes are illustrated in Fig. 7. Notice how iteration $n = 0$ is a simple equilateral triangle and iteration $n = 2$ begins to take shape of a snowflake. The increase of the surface area for every increment in iteration is clearly noticeable, especially when comparing between iteration $n = 0$ and iteration $n = 2$. The initial length of one of the sides of the equilateral triangle from iteration $n = 0$ is 18 mm. The side lengths of the other smaller triangles in the following iterations can be found by using Eq. (2) previously introduced.

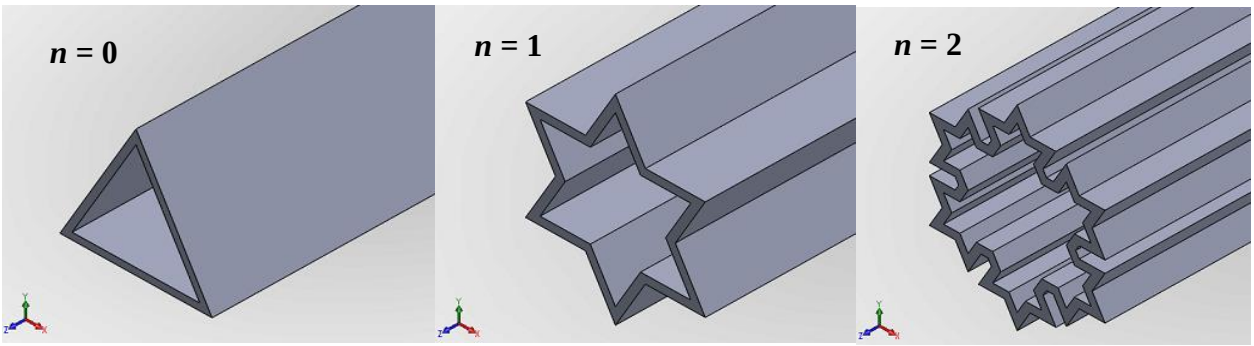

Figure 7 Modified Koch Snowflake Pipes

Computational Methodology

Governing Equations

The numerical simulations used to analyze the modified heat exchanger's thermal performance were performed in ANSYS Fluent 17.1. The Reynolds Averaged Navier-Stokes (RANS) were utilized in this analysis as turbulent flow was considered. The equations governing the fluid flow

and heat transfer are discussed into more detail below. The continuity and momentum equation are shown in Eq. (19) and Eq. (20), respectively.

$$\frac{\partial \rho}{\partial t} + \nabla \cdot (\rho \vec{v}) = S_m \tag{19}$$

$$\frac{\partial \rho}{\partial t}(\rho \vec{v}) + \nabla \cdot (\rho \vec{v} \vec{v}) = -\nabla p + \nabla \cdot (\bar{\bar{\tau}}) + \rho \vec{g} + \vec{F} \tag{20}$$

In the continuity equation, ρ is the density of the fluid, v the velocity, and S_m is the mass added to the continuous phase. In the momentum equation, p is the static pressure, $\bar{\bar{\tau}}$ is the stress tensor displayed in Eq. (21), and $\rho\vec{g}$ and $\vec{F}$ are the gravitational body forces and external body forces, respectively. The stress tensor previously mentioned is given by

$$\bar{\bar{\tau}} = \mu[(\nabla \vec{v} + \nabla \vec{v}^T)] - \frac{2}{3} \nabla \cdot \vec{v} I \tag{21}$$

where μ is the molecular viscosity, I the unit tensor, and the second term on the right-hand side is the effect of volume dilation.

Turbulence Model

As the flow in most industrial heat exchangers applications is turbulent, a turbulence model was utilized in the computational simulations. Specifically, the realizable k-ε turbulent model proposed by Shih et al. was selected for this study [18]. The k-ε turbulence model has been extensively validated for a wide range of flows [19]. The modeled transport equations for k and ε in the realizable k-ε model can be seen in Eq. (22) and Eq. (23), respectively.

$$\frac{\partial}{\partial t}(pk) + \frac{\partial}{\partial x_j}(pku_j) = \frac{\partial}{\partial x_j}\left[\left(\mu + \frac{\mu}{\sigma_\varepsilon}\right)\frac{\partial \varepsilon}{\partial x_j}\right] + G_k + G_b - \rho\varepsilon - Y_M + S_k \tag{22}$$

and

$$\frac{\partial}{\partial t}(p\varepsilon)+\frac{\partial}{\partial x_j}(p\varepsilon u_j)=\frac{\partial}{\partial x_j}\left[\left(\mu+\frac{\mu}{\sigma_\varepsilon}\right)\frac{\partial \varepsilon}{\partial x_j}\right]+\rho C_1 S\varepsilon-\rho C_2\frac{\varepsilon^2}{k+\sqrt{\upsilon\varepsilon}}+C_{1\varepsilon}\frac{\varepsilon}{k}C_{3\varepsilon}G_b+S_\varepsilon \quad (23)$$

where

$$C_1=max\left[0.43,\frac{\eta}{\eta+5}\right],\qquad \eta=S\frac{k}{\varepsilon}\qquad S=\sqrt{2S_{ij}S_{ij}} \quad (24)$$

In these equation, G_k represents the generation of turbulence kinetic energy due to mean velocity gradients, G_b is the generation of turbulent kinetic energy due to buoyancy, Y_M is the contribution of the fluctuating dilatation in compressible turbulence to the overall dissipation rate. C_2 and $C_{1\varepsilon}$ are constants. Then, σ_k and σ_ε are the turbulent Prandtl numbers for k and ε, respectively. S_k and S_ε are user defined source terms. The model for turbulent eddy viscosity is presented in the following Eq. (25).

$$\mu_t=\rho C_\mu\frac{k^2}{\varepsilon} \quad (25)$$

The C_μ in the realizable k-ε models is not constant and calculated as seen in Eq. (26)

$$C_\mu=\frac{1}{A_0+A_s\frac{kU^*}{\varepsilon}} \quad (26)$$

where,

$$U^*=\sqrt{S_{ij}S_{ij}+\tilde{\Omega}_{ij}\tilde{\Omega}_{ij}} \quad (27)$$

and,

$$\tilde{\Omega}_{ij}=\Omega_{ij}-2\varepsilon_{ijk}\omega_k \quad (28)$$

$$\Omega_{ij}=\overline{\Omega_{ij}}-2\varepsilon_{ijk}\omega_k \quad (29)$$

where $\overline{\Omega_{ij}}$ is the mean rate-of-rotation tensor viewed on a moving reference frame with an angular velocity ω_k. The model constants A_0 and A_s are given by

$$A_0 = 4.04, \quad A_s = \sqrt{6}\cos\phi$$

where finally,

$$\phi = \frac{1}{3}\cos^{-1}\left(\sqrt{6}W\right), \qquad W = S_{ij}S_{ik}S_{ki}, \quad \tilde{S} = \sqrt{S_{ij}S_{ij}}, \quad S_{ij} = \frac{1}{2}\left(\frac{\partial u_j}{\partial x_i} + \frac{\partial u_i}{\partial x_j}\right) \tag{30}$$

and the constant variables of the model are:

$$C_{1\varepsilon} = 1.44, \quad C_2 = 1.9, \quad \sigma_k = 1.0, \quad \sigma_\epsilon = 1.2$$

Heat Transfer Model

ANSYS Fluent is also capable of solving heat transfer through the energy equation. Heat transfer within the fluid and/or a solid can be solved simultaneously. A model of a DPHE is a perfect example of the capabilities of this software. Where convection is occurring within a fluid, and conduction through the solid pipes. To include heat transfer in the model, certain parameters must be taken into consideration. Such as thermal boundary conditions and material properties that govern heat transfer, which may vary with temperature. The energy equation being solved for a turbulent model is shown in Eq. (31).

$$\frac{\partial}{\partial t}(\rho E) + \frac{\partial}{\partial x_i}[u_i(\rho E + p)] = \frac{\partial}{\partial x_j}\left(k_{eff}\frac{\partial T}{\partial x_j} + u_i\left(\tau_{ij}\right)_{eff}\right) + S_h \tag{31}$$

where $(\tau_{ij})_{eff}$ is the deviatoric stress sensor, defined in Eq. (32). *E* is the total energy as seen in Eq. (33), and k_{eff} is the effective thermal conductivity shown in Eq. (35),

$$\left(\tau_{ij}\right)_{eff} = \mu_{eff}\left(\frac{\partial u_j}{\partial x_i} + \frac{\partial u_i}{\partial x_j}\right) - \frac{2}{3}\mu_{eff}\frac{\partial u_k}{\partial x_k}\delta_{ij} \tag{32}$$

$$E = h - \frac{p}{\rho} + \frac{v^2}{2} \tag{33}$$

where *h* for an incompressible flow is defined as seen in Eq. (34),

$$h = \sum_j Y_j h_j + \frac{p}{\rho} \tag{34}$$

and for realizable k-ε models, the effective thermal conductivity is given by

$$k_{eff} = k + \frac{c_p \mu_t}{Pr_t} \tag{35}$$

where k is the thermal conductivity, and the default value of the turbulent Prandtl number is 0.85. The previously described governing equations for continuity, momentum, and energy are the general version that can be applicable to any turbulent model. Depending on the application, some of the terms are not taken into consideration. By establishing assumptions to the model, it is possible to simplify these equations. In this study the assumptions taken were:

1. Heat exchangers usually operate for long periods of time with no change in their operating conditions. Therefore, they can be modeled as steady-state flow devices.
2. The fluid streams experience little to know change in their velocities and elevations, and thus the kinetic and potential energy changes are negligible.
3. The fluid (water) being used is incompressible and thus the density can be assumed to be constant.
4. Axial heat conduction along the pipe is usually insignificant, and can be considered negligible in most theoretical analysis. However, it is taken into account in the computational model.
5. The outer surface of the heat exchanger is assumed to be perfectly insulated, so there is no heat loss to the surrounding medium, and heat transfer occurs between the two fluids only. In this manner, the rate of heat transfer of the hot fluid is equal to that of the cold fluid.
6. The working fluid, single phase water, was assumed to have temperature-dependent thermophysical and rheological properties.

With these assumptions taken into consideration, the simplified continuity Eq. (36), momentum Eq. (37), and energy Eq. (38) equations are displayed as follows. Assuming a steady-state, and temperature dependent thermophysical and rheological properties, the continuity equation, in its reduced form is

$$\nabla(\rho\vec{v}) = 0 \tag{36}$$

Similarly, assuming a steady-state, temperature dependent properties, and negligible gravitational body forces, the momentum equation can be reduced to

$$\nabla(\rho\vec{v}\vec{v}) = -\nabla \mathrm{p} + \nabla(\bar{\bar{\tau}}) \tag{37}$$

where the stress tensor is given by

$$\bar{\bar{\tau}} = \mu\nabla\vec{v} \tag{38}$$

Once again assuming a steady-state, temperature dependent properties, and the energy equation can be simplified to

$$\nabla\left(\vec{v}(\rho E + p)\right) = \nabla\left(k\nabla T + \left(\bar{\bar{\tau}}_{eff}\vec{v}\right)\right) \tag{39}$$

where the total energy is given by

$$E = h - \frac{p}{\rho} + \frac{v^2}{2} \tag{40}$$

Neglecting the flow work and kinetic energy terms, the energy equation simplifies to

$$\nabla\left(\vec{v}(\rho h)\right) = \nabla\left(k\nabla T + \left(\bar{\bar{\tau}}_{eff}\vec{v}\right)\right) \tag{41}$$

where the enthalpy is defined as

$$h = c_p T \tag{42}$$

Mesh Generation

The DPHE being studied, was discretized to employ the finite volume method. The governing equations for mass, momentum and energy are solved on these set of control volumes. The quality of the mesh in a numerical simulation is of critical importance. The mesh structure and refinement play an important role in obtaining a high degree of accuracy, and obtaining the solution in a reasonable amount of computational time. A balance between the two will provide an optimum mesh.

A series of steps were taken to create the mesh of four different models: the traditional DPHE with circular pipe, and iterations $n = 0$, $n = 1$, and $n = 2$ of the modified Koch Snowflake DPHE. All the geometries were imported to ANSYS Design Modeler from SolidWorks. They were simplified, defeatured, and translated to have a consistent orientation. For the traditional DPHE with circular pipe, a structured hexahedral mesh with a swept method was implemented as seen in Fig. 8. The mesh was refined locally using sizing and inflation layers to properly capture the boundary layer, a cross-sectional view of the mesh is illustrated in Fig. 9. The calculated height of the first layer thickness, using the appropriate y+ values, was taken into consideration in the mesh generation, as seen in Fig. 10. The hexahedral mesh with a swept method was set for 250 divisions along the z-axis as illustrated in Fig. 11. The total number of elements produced was approximately 1.3 million.

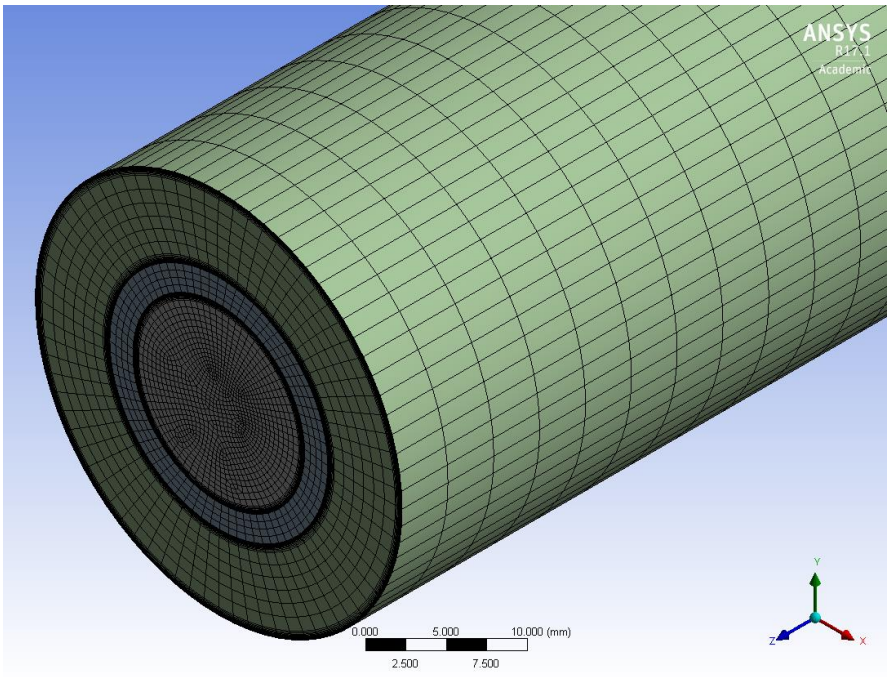

Figure 8 Mesh Structure for Cylindrical Pipe DPHE

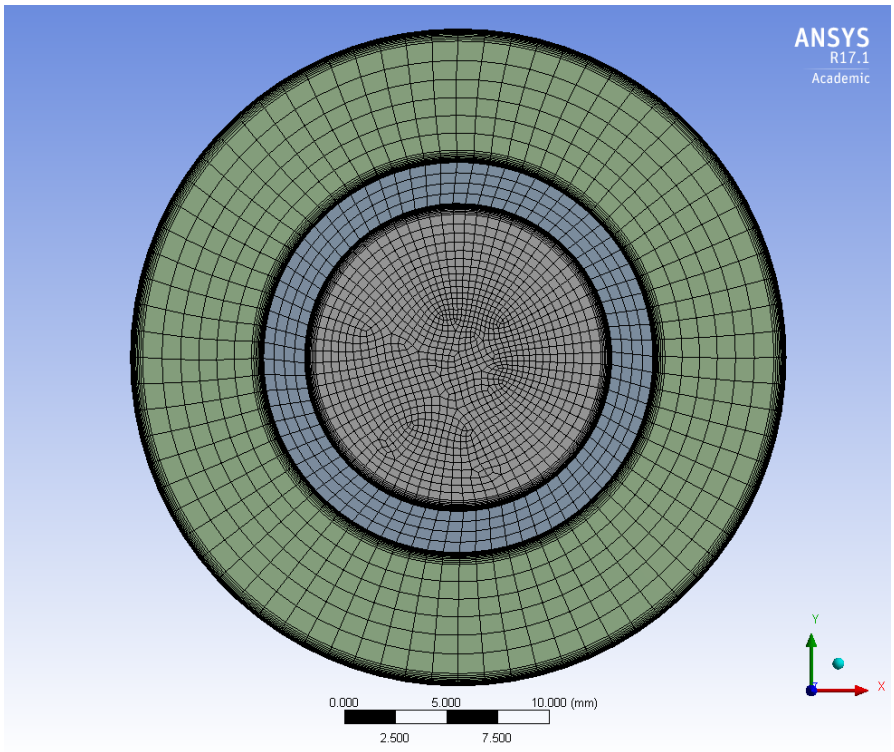

Figure 9 Mesh Structure of Circular Cross-Section

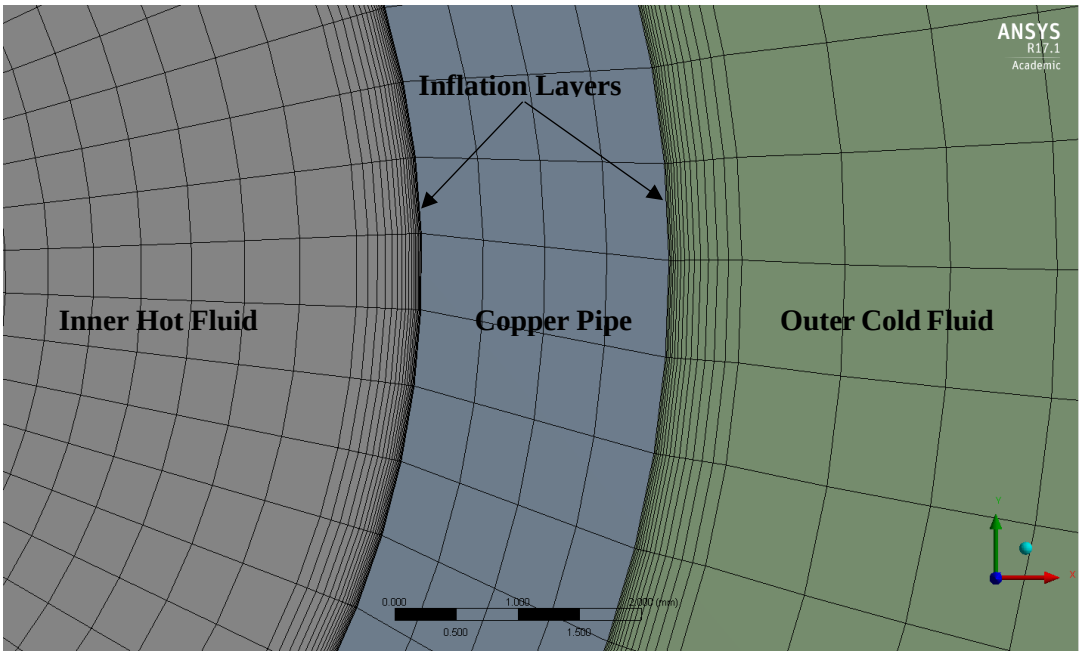

Figure 10 Zoomed in View of Inflation Layers to Capture Boundary Layer

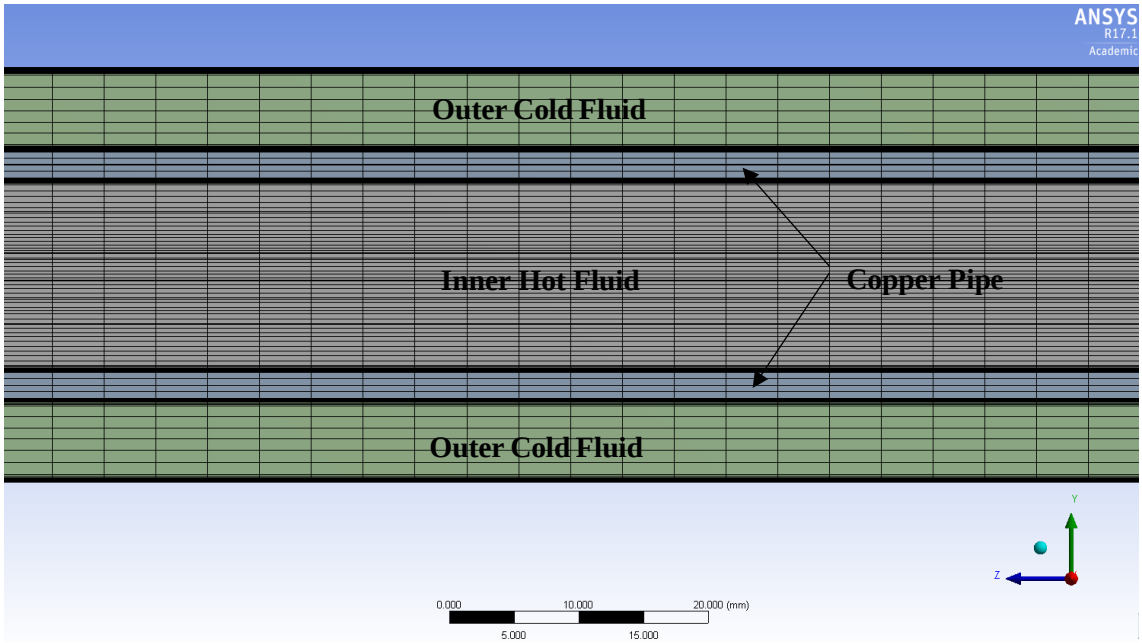

Figure 11 Mesh Structure along Z-Axis

The mesh for the zeroth to the second iteration of the Koch Snowflake DPHE were generated in a similar manner. They consist of mostly hexahedral and wedge elements, which are highly encouraged for a mesh in computational fluid analysis. The corresponding first layer thickness for each fractal iteration was also calculated and the proper inflation layer for the fluid domains was added. The mesh structures of the cross-section of the Koch Snowflake fractal for iteration $n = 0$ is illustrated in Fig. 12, iteration $n = 1$ in Fig. 13, and iteration $n = 2$ in Fig. 14.

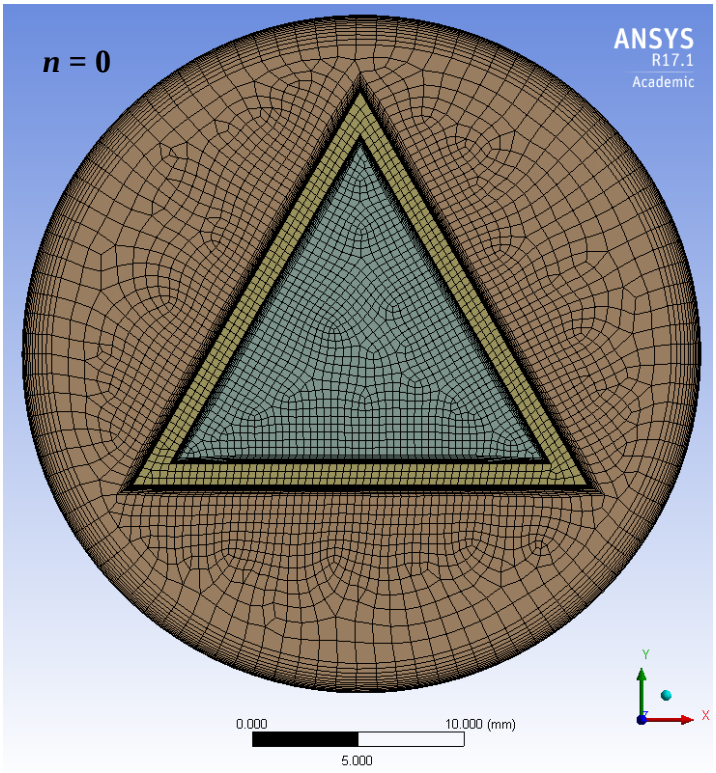

Figure 12 Mesh Structure of Koch Snowflake DPHE Cross-Section Iteration $n = 0$

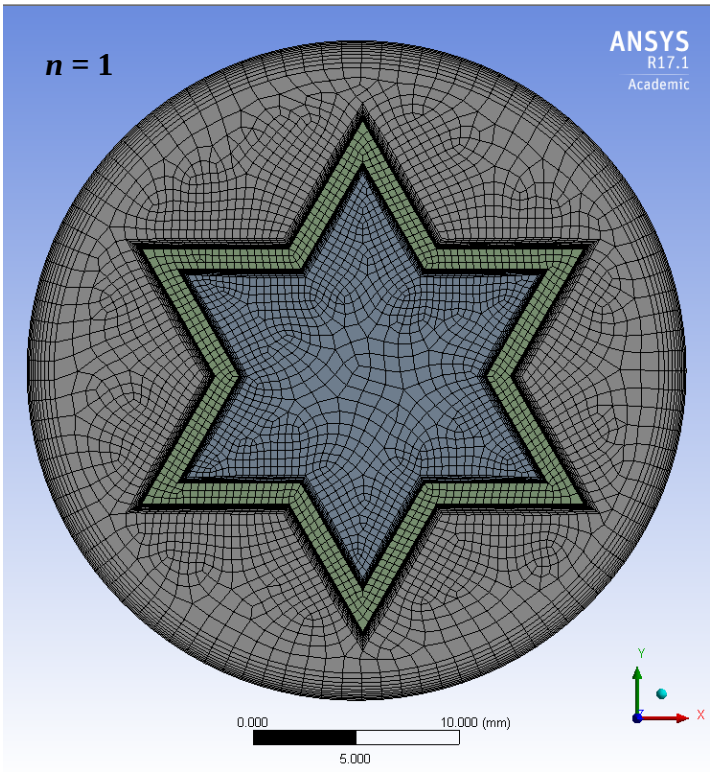

Figure 13 Mesh Structure of Koch Snowflake DPHE Cross-Section Iteration *n* = 1

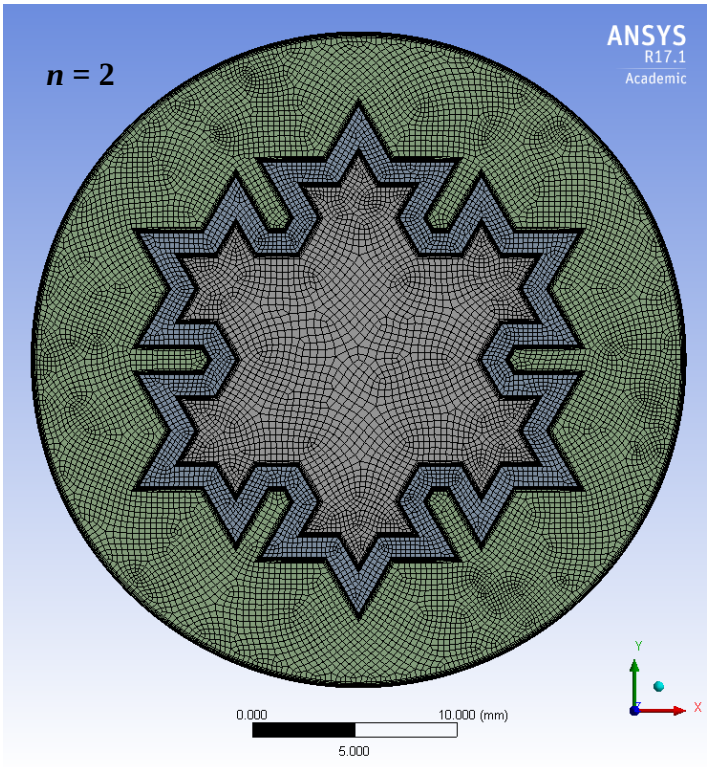

Figure 14 Mesh Structure of Koch Snowflake DPHE Cross-Section Iteration *n* = 2

The quality of the mesh has a significant impact on the accuracy and stability of the numerical solution. Checking for mesh quality is essential in numerical solutions. To check for mesh quality several mesh metrics are available. One of the most common methods of checking the quality of the mesh is the cell skewness. The skewness is defined as the difference between the shape of the cell and the shape of the equilateral cell of equivalent volume. Highly skewed cell can decrease the accuracy of the numerical solution. A general rule of thumb for checking skewness is the following: if the skewness value is 0-0.25 (excellent), 0.25-0.50 (very good), 0.50-0.80 (good), 0.80-0.94 (acceptable), 0.95-0.97 (bad), and 0.98-1.00 (unacceptable). The skewness and number of elements for each geometry being studied was recorded and can be seen in Table 2.

Table 2 Skewness and Number of Elements for Each Geometry

Geometry	Number of Elements	Skewness (Max)	Skewness (Average)
Traditional	1,311,000	0.49	0.05
Iteration 0	1,885,750	0.72	0.20
Iteration 1	1,982,000	0.71	0.31
Iteration 2	4,865,500	0.70	0.21

Boundary Conditions

In a numerical simulation, the conditions that are observed in a real-life experiment are adopted. The initial fluid and thermal boundary conditions are described in this section. The model consists of two inlets and two outlets. The inlets consider an inlet velocity and the outlets a pressure outlet. Uniform inlet velocities were utilized. The magnitude of the inlet velocity was changed to achieve prescribed inlet Reynolds numbers. It should be noted that in order to calculate the Reynolds number, a hydraulic diameter had to be calculated for each of the fractal heat exchangers due to their non-circular cross-sectional geometries. Simulations, for a range of Reynolds numbers from

10000 to 40000 were performed in increments of 5000. Note that this Reynolds number range corresponds to a turbulent flow regime. The pressure outlets are the same throughout all models considering an atmospheric (zero-gauge) pressure outlet at an ambient temperature of 30°C (303 K). The working fluid, in the inner pipe as well as in the annular space, was assumed to be incompressible and single phase water. The inner pipe was composed of copper with constant thermophysical properties. It was assumed that there was no velocity slip at all walls. The outer pipe, composed of aluminum, was assumed to be perfectly insulated. The inlet temperatures were 20°C for the cold fluid and 60°C for the hot fluid. The heat-exchangers were assumed to operate in the counter-flow configuration. An overview of the boundary conditions imposed to the DPHE are illustrated in Fig. 15.

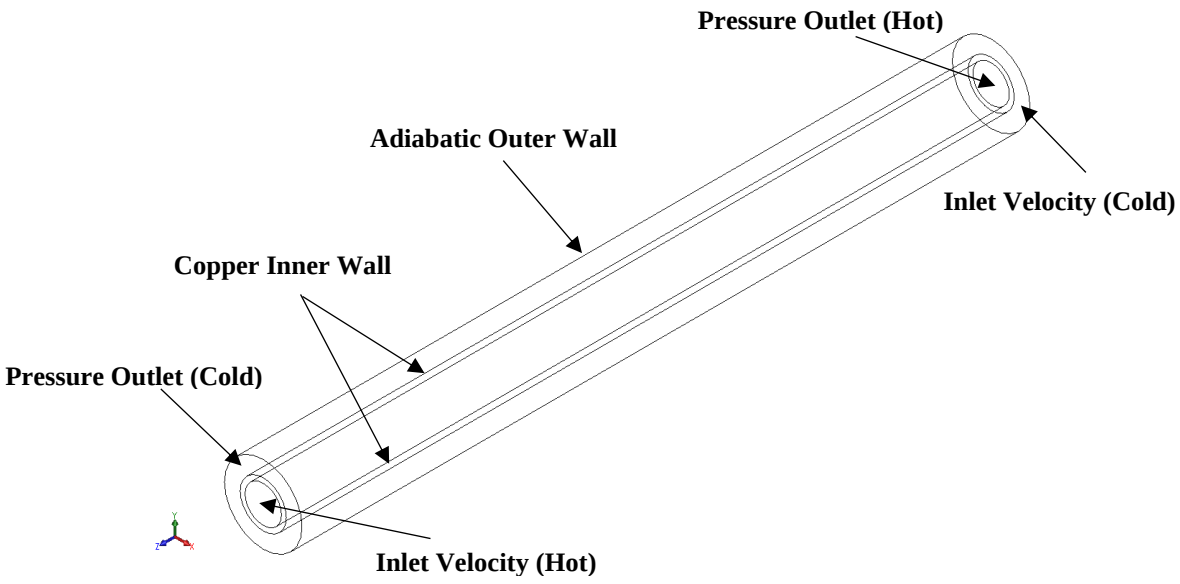

Figure 15 Overview of Initial Boundary Conditions

Solution Methods

Pressure-velocity coupling was achieved via the SIMPLE (Semi-Implicit Method for Pressure Linked Equations) method which uses a relationship between velocity and pressure corrections to enforce mass conversation and to obtain the pressure field.

The CFD software stores discrete values of field variables at cell centers. However, face values are required for the convective term and must be interpolated from the cell center values. This was accomplished via the QUICK (Quadratic Upstream Interpolation for Convective Kinematics) scheme due to the use of hexahedral elements. A second order scheme was utilized to interpolate pressure values at cell faces. Gradients required to construct scalar values of field variables at cell faces as well as for determining secondary diffusion terms and velocity derivatives were calculated according to the Least Squares Cell-Based method.

The pressure based solver utilizes under-relaxation to control the update of computed variables at each iteration. Under-relaxation factors for pressure and momentum were 0.3 and 0.7 and for energy was 0.9.

Validation

The numerical simulation results were compared to theoretical correlations for validation of the model. The theory provides correlations that are useful for solving fluid and thermal characteristics of a system. The theoretical equations to solve for pressure drop, friction factor, and Reynolds number were obtained from Çengel et al. [1]. The pressure drop was analytically calculated for the traditional DPHE using the theoretical correlations and compared to the numerical simulation outlet pressures.

The pressure drop for the analytical solution is given by Eq. (43).

$$P_L = f\frac{L}{D_h}\frac{\rho v^2}{2} \tag{43}$$

where f is the friction factor obtained using the the Haaland equation, Eq. (44), which is an approximation of the Colebrook-White equation that iteratively solves the Darcy-Weisbach friction factor formula, v is velocity calculated by Eq. (45) and L is the length of the pipe.

$$\frac{1}{\sqrt{f}} = -1.8\log\left[\left(\frac{\frac{\epsilon}{D_h}}{3.7}\right)^{1.11} + \frac{6.9}{Re}\right] \tag{44}$$

$$v = \frac{Re\ \nu_k}{D_h} \tag{45}$$

In the equation above ε is the pipe roughness, ν_k the kinematic viscosity, and D_h the hydraulic diameter calculated by Eq. (46).

$$D_h = \frac{4A}{P} \tag{46}$$

The hydraulic diameter was of critical importance in the analytical solution since the cross-section area, A, and the perimeter, P, of the Koch Snowflakes varied per iteration. This resulted in modified velocities to achieve a constant Reynolds number. For the validation, only the equations for a circular cross section were used. The analytical pressure drop for the inlet of the hot fluid was found to be in good agreement with the numerical solutions as illustrated in Fig.16. A close agreement can also be observed for the cold fluid inlet pressure as illustrated in Fig. 17.

Table 3 Hot Fluid Inlet Pressure Numerical and Theoretical Comparison

Reynolds Number	Analytical (Pa)	Simulation (Pa)	% Error
10000	461.4	469.5	1.8
15000	932.9	919.5	1.4
20000	1542.9	1502.5	2.6
25000	2284.3	2189.9	4.1
30000	3151.8	3004.9	4.7
35000	4141.4	3926.2	5.2
40000	2550.1	4944.9	5.8

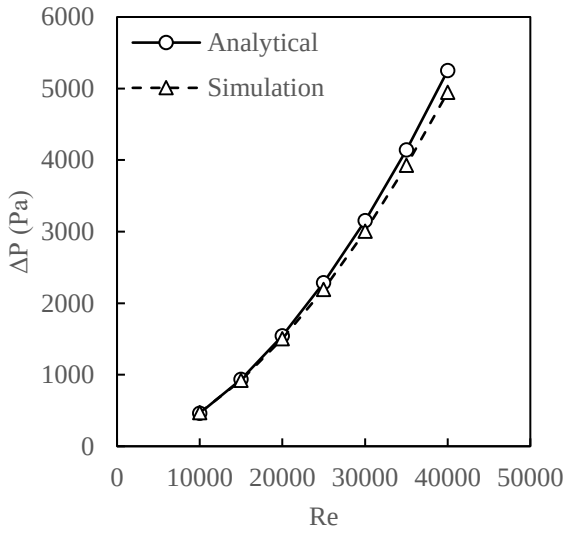

Figure 16 Hot Fluid Pressure Drop for Various Reynolds Numbers Comparison

Table 4 Cold Fluid Inlet Pressure Numerical and Theoretical Comparison

Reynolds Number	Analytical (Pa)	Simulation (Pa)	% Error
10000	709.2	846.9	19.4
15000	1434.2	1668.8	16.4
20000	2372.7	2702.8	13.9
25000	3513.5	3935.6	12.0
30000	4848.8	5300.9	9.3
35000	6372.6	6837.7	7.3
40000	8080.2	8608.5	6.5

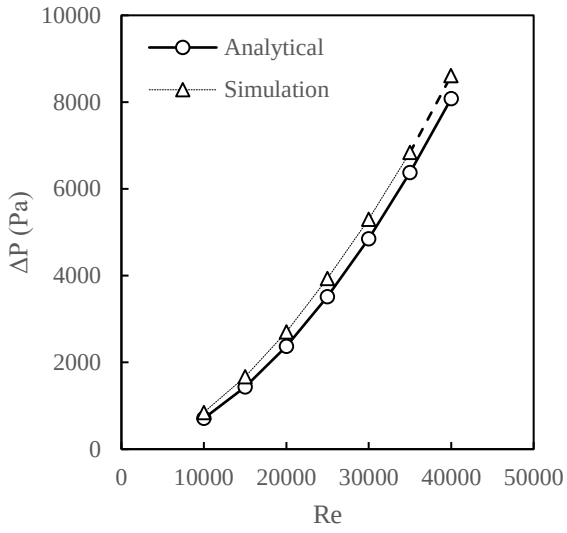

Figure 17 Cold Fluid Pressure Drop for Various Reynolds Numbers Comparison

Verification

To verify that the mesh was grid-independent, meaning that the mesh structure obtained is the suitable one for this study, a grid sensitivity analysis was performed. A fine enough mesh is required for an accurate solution, but at the same time computational time is of essence. The goal of a grid-independence study is to monitor an important solution variable, in this case the inlet static pressure, and ensure that the solution variable does not change with further refinement of the mesh density. The pressure drop as a function of the number of cells can be seen in Fig. 18. It is seen that after approximately 1.3 million elements the inlet static pressure (gage) is approaching an asymptotic value. Further increasing the density of the mesh would increase computational time but would not greatly impact the accuracy of the solution. It should be noted that a tradeoff is always made between computational time and what is deemed as an acceptable level of accuracy. The number of cells in a computational domain is directly related to the computational time required.

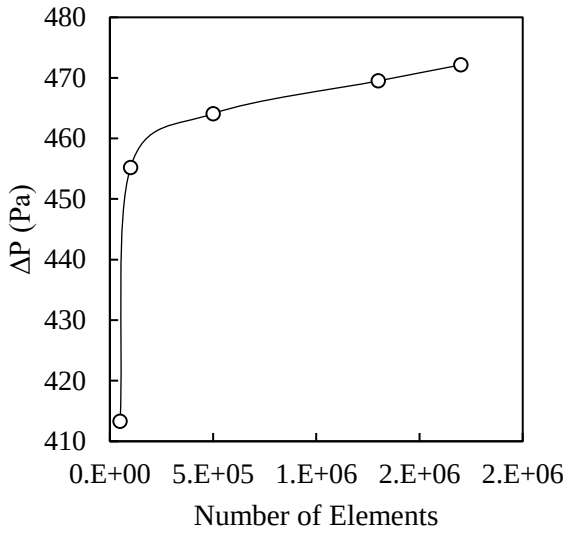

Figure 18 Verification of Grid-Independence

Results

Having validated a computational model of a traditional double-pipe heat exchanger with a theoretical solution and also verifying the solution for grid independence, a computational model of a fractal double-pipe heat exchanger can be examined. The surface area of a heat exchanger with a fractal cross-section in accordance with the Koch snowflake fractal pattern is highly-dependent upon fractal iteration. An approximation of the inner pipe surface area for the traditional as well as for the first three iterations of the Koch snowflake fractal pattern can be seen in the table below.

Table 5 Heat Transfer Surface Area of Inner Pipe

Geometry	Surface Area (mm^2)
Traditional	47000
Iteration 0	54000
Iteration 1	72000
Iteration 2	96000

Overall Heat Transfer Coefficient

The heat transfer coefficients for the hot and cold fluids were obtained from the simulations and used to evaluate the total thermal resistance using Eq. (10). The conduction resistance in the inner pipe wall was assumed to be negligible. This was because the inner pipe was composed of copper of a relatively thin thickness. As the thickness was relatively small, and the thermal conductivity of copper is relatively high, there is a fairly negligible conduction resistance for the inner pipe wall. On the other hand the increase in surface area, associated with increases in fractal iteration, directly impacts the overall heat transfer coefficient. A plot of the overall heat transfer coefficient as a function of inlet Reynolds number and fractal iteration can be seen in Fig. 19. As expected, an increase in the inlet Reynolds number resulted in an increase in the overall heat transfer coefficient. As the number of fractal iterations increased, so did the overall heat transfer coefficient, largely due to the increase in available surface area for convective heat transfer.

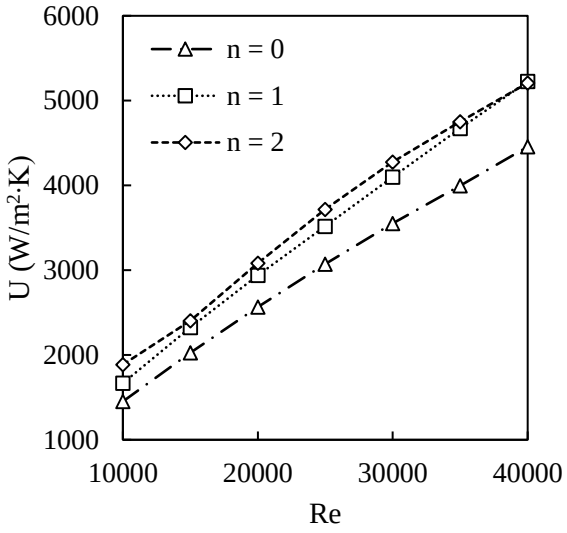

Figure 19 Overall Heat Tranfer Coefficient as a Function of Reynolds number

When compared with a traditional double-pipe heat exchanger with a circular cross-section, a 30% increase in the overall heat transfer coefficient is achieved with a cross-section in accordance with the second iteration of the Koch snowflake fractal pattern for an inlet Reynolds number of 10,000.

As the heat transfer rate is directly proportional to the overall heat transfer coefficient and the available surface area, it was anticipated that the heat transfer would increase with the number of fractal iterations. A double-pipe heat exchanger with a cross-section in accordance with the second iteration of the Koch snowflake fractal pattern significantly outperforms a traditional double-pipe heat exchanger with a circular cross-section.

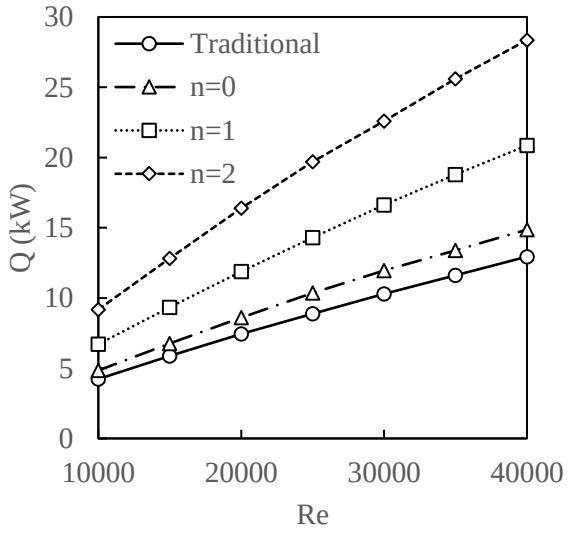

Figure 20 Heat Transfer Rate as a Function of Reynolds Number

Compared with a traditional heat exchanger, an increase in the heat transfer rate of 16%, 52%, and 75% can be achieved with cross-sections in accordance with the zeroth, first, and second iteration of the Koch snowflake fractal pattern respectively.

Effectiveness and NTU

As the Number of Transfer Units (NTU) primarily identifies the size of a heat exchanger, it was expected that NTU would increase with fractal iteration due to the increase in surface area. However, it should also be noted that the NTU is also a function of the overall heat transfer coefficient and the minimum heat capacity rate. The overall heat transfer coefficient and heat capacity rates are a function of the inlet Reynolds number. As the Reynolds number increases, the number of transfer units decreases.

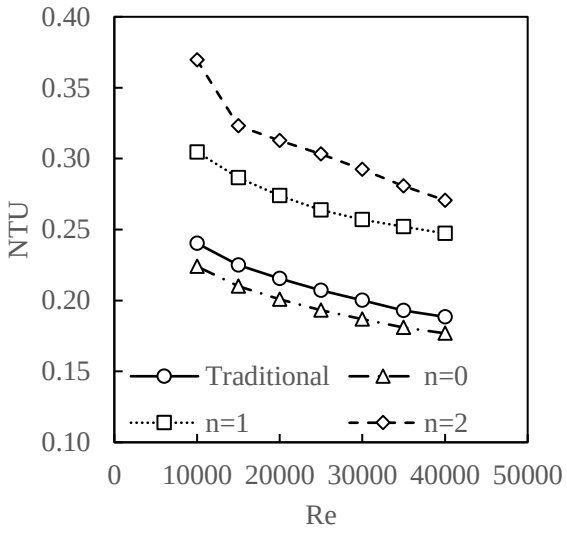

Figure 21 Variation of NTU with Reynolds Number for DPHE

The most important performance metric is the heat exchanger's effectiveness. The effectiveness shows the actual heat transfer rate compared to the maximum possible heat transfer rate. The higher the actual heat transfer rate the higher the effectiveness. The heat exchanger with a cross-section in accordance with the second fractal iteration of the Koch snowflake fractal pattern resulted in the greatest heat transfer effectiveness. It should be noted that the zeroth iteration, a triangular cross-section, offers similar performance as the traditional circular cross-section which can largely be attributed to their similar surface areas. However, it should also be noted that a circular cross-

section is the most desirable from the perspective of minimizing pumping power. It was not the goal of this analysis to analyze the hydrodynamic performance but rather the thermal performance of heat exchangers with fractal geometries.

Contour plots of fluid temperature can be found in the Appendix for both the traditional as well as the Koch snowflake inspired fractal heat exchangers.

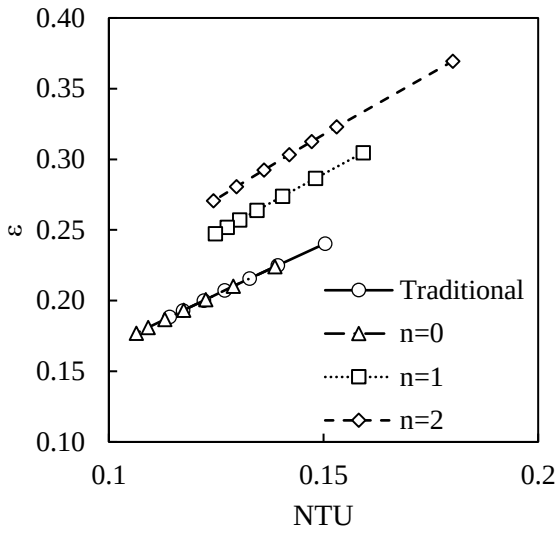

Figure 22 Effectiveness as a Function of NTU

CONCLUSIONS

A thermal performance of a traditional double-pipe heat exchanger with a circular cross-section was compared to the performance of double-pipe heat exchangers with cross-section in accordance with the first three fractal iterations of the Koch snowflake pattern. The computational models were validated with a theoretical model for pressure drop and verified for grid independence through a mesh sensitivity analysis. The benefit of the use of the Koch snowflake design is that an increase in surface area can be achieved without impacting package volume. Thus, heat exchangers with fractal designs have significantly higher surface areas per unit package volume when compared with traditional heat exchangers. The increase in surface area associated with each fractal iteration resulted in higher overall heat transfer coefficients and heat transfer rates. In addition, the effectiveness of the fractal heat exchangers was greater than that of the traditional heat exchanger, regardless of iteration. As the number of fractal iterations increased, the effectiveness also increased. It is hypothesized that further iterations may result in an additional increase in effectiveness. Future studies may need to examine the tradeoff between increase in heat transfer and increasing in pumping power requirements.

REFERENCES

[1] Y. A. Cengel and G. J. Afshin, Heat and Mass Transfer: Fundamentals & Applications, New York: McGraw-Hill, 2011.

[2] E. A. Bergles, "The Imperative to Enhance Heat Transfer," in *Heat Transfer Enhancement of Heat Exchangers*, Springer Netherlands, 1999, pp. 13-29.

[3] M. Omidi, M. Farhadi and M. Jafari, "A Comprehensive Review on Double Pipe Heat Exchangers," *Applied Thermal Engineering*, pp. 1075-1090, 2017.

[4] Z. Huang, Y. Hwang, V. Aute and R. Radermacher, "Review of Fractal Heat Exchangers," in *International Refrigeration and Air Conditioning Conference*, West Lafayette, 2016.

[5] G. H. Ibrahim, "Experimental and CFD Analysis of Turbulent Flow Heat Transfer in Tubular Exchanger," *International Journal of Engineering and Applied Sciences*, pp. 18-24, 2014.

[6] H. Van der Vyer, J. Dirker and P. M. Meyer, "Validation of a CFD Model of a Three-Dimensional Tube-in-Tube Heat Exchanger," in *Third International Conference on CFD in the Minerals and Process Industries*, Melbourne, 2003.

[7] K. Arslan, "Three-Dimensional Numerical Investigation of Turbulent Flow and Heat Transfer Inside a Horizontal Semi-Circular Cross-Sectioned Duct," *Thermal Science*, pp. 1145-1158, 2014.

[8] V. Kumar, S. Saini, M. Sharma and K. Nigam, "Pressure Drop and Heat Transfer Study in Tube-in-Tube Helical Heat Exchanger," *Chemical Engineering Science,* pp. 4406-4416, 2006.

[9] D. Bhanuchandrarao, C. M. Ashok, Y. Krishna, V. S. Rao and H. Krishna, "CFD Analysis and perfromance of Parallel and Counter Flow in Concentric Tube Heat Exchangers," *International Journal of Engineering Reasearch & Technology,* pp. 2782-2792, 2013.

[10] W.-L. Chen and W.-C. Dung, "Numerical Study on Heat Transfer Characteristics of Double Tube Heat Exchangers with Alternating Horizontal or Vertical Oval Cross Section Pipes as Inner Tubes," *Energy Conversion and Management,* pp. 1574-1583, 2008.

[11] R. Bhadouriya, A. Agrawal and S. Prabhu, "Experimental and Numerical Study of Fluid Flow and Heat Transfer in an Annulus of Inner Twisted Square Duct and Outer Circular Pipe," *International Journal of Thermal Sciences,* pp. 96-109, 2015.

[12] P. J. Meyer and H. Van der Vyver, "Heat Transfer Characteristics of a Quadratic Koch Island Fractal Heat Exchanger," *Heat Transfer Engineering,* pp. 22-29, 2005.

[13] P. Wang, M. Yang, Z. Wang and Y. Zhang, "A New Heat Transfer Correlation for Turbulent Flow of Air With Variable Properties in Noncircular Ducts," *Journal of Heat Transfer,* pp. 1-8, 2014.

[14] S. Kumar, K. V. Karanth and K. Murthy, "Numerical Study of Heat Transfer in a Finned Double Pipe Heat Exchanger," *World Journal of Modelling and Simulation,* pp. 43-54, 2015.

[15] M. V. Hameed and B. M. Essa, "Experimental and Numerical Investigation to Evaluate the Performance of Triangular Finned Tube Heat Exchanger," *International Journal of Energy and Environment,* pp. 553-566, 2015.

[16] B. B. Verma and S. Kumar, "CFD Analysis and Optimization of Heat Tranfer in Double Pipe Heat Exchanger with Helical-Tap Inserts at Annulus of Inner Pipe," *Journal of Mechanical and Civil Engineering,* pp. 17-22, 2016.

[17] M. Hashenmian, S. Jafarmadar and H. S. Dizaji, "A Comprenhensive Numerical Study on Multi-Criteria Design Analyses in a Novel Form (Conical) of Double Pipe Heat Exchanger," *Applied Thermal Engineering,* pp. 1228-1237, 2016.

[18] H. T. Shih, W. W. Liou, Z. Yang and J. Zhu, "A New k-ε Eddy-Viscosity Model for High Reynolds Number Turbulent FLows - Development and Validation," *Computer Fluids,* pp. 227-238, 1995.

[19] ANSYS, ANSYS Fluent Theory Guide, Canonsburg: ANSYS, Inc., 2016.

APPENDICES

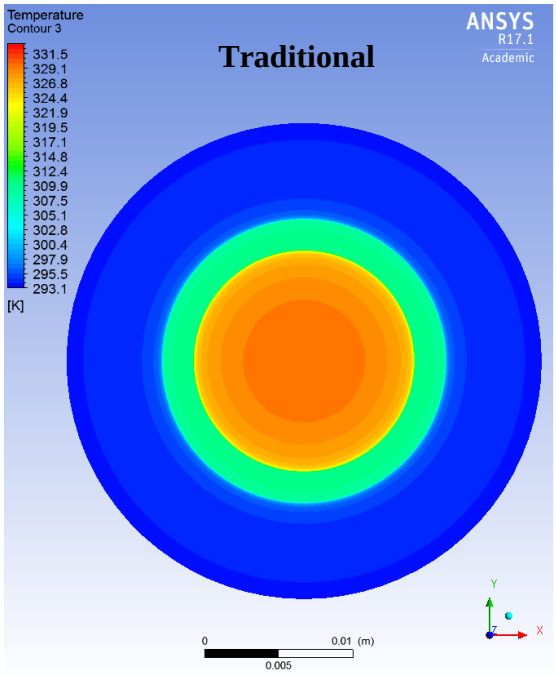

Figure 23 Traditional Pipe Cross Section Temperature Contour

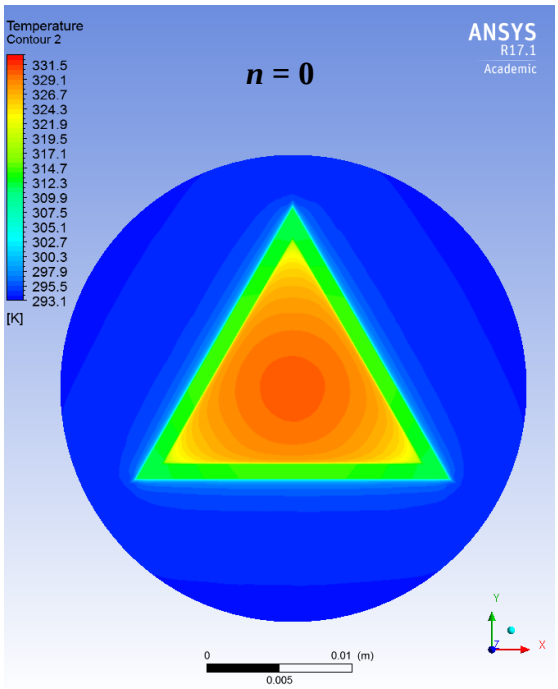

Figure 24 Iteration *n* = 0 Pipe Cross Section Temperature Contour

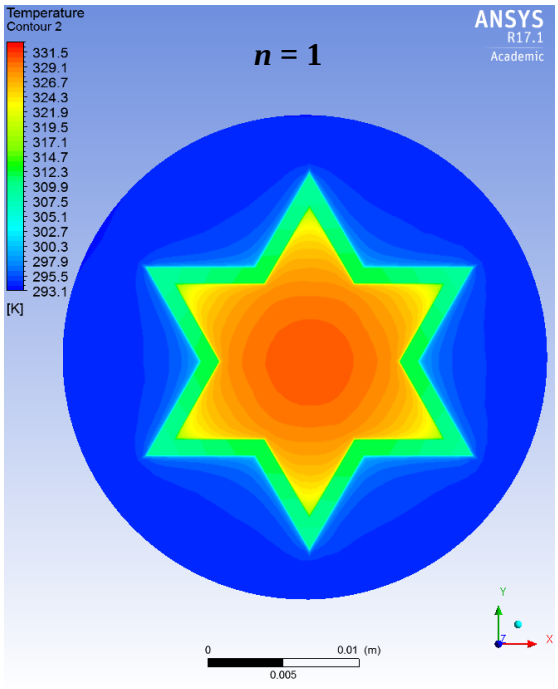

Figure 25 Iteration *n* = 1 Pipe Cross Section Temperature Contour

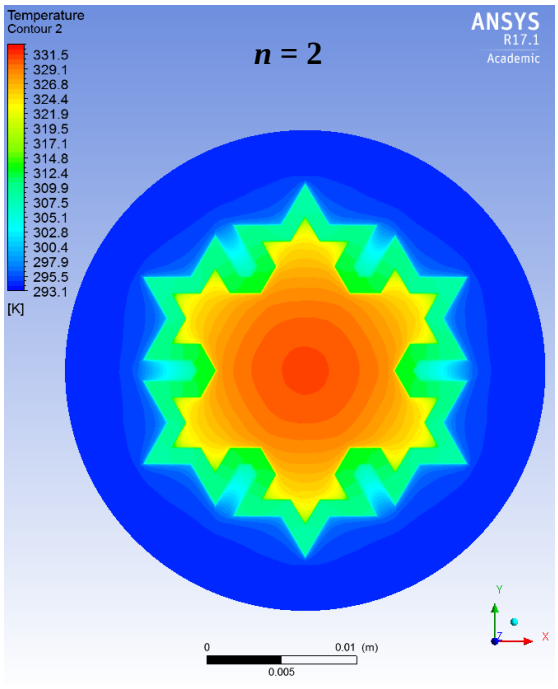

Figure 26 Iteration *n* = 2 Pipe Cross Section Temperature Contour

Re = 10,000

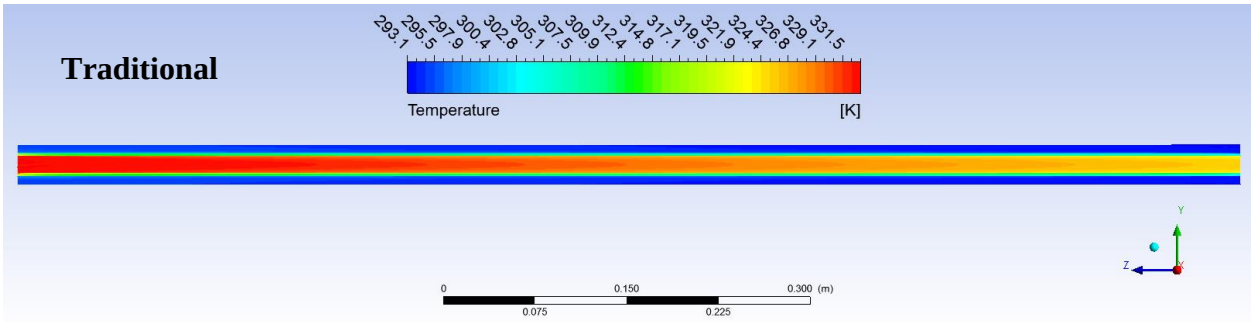

Figure 27 Temperature Contour along Z-Axis Traditional Pipe at Re = 10000

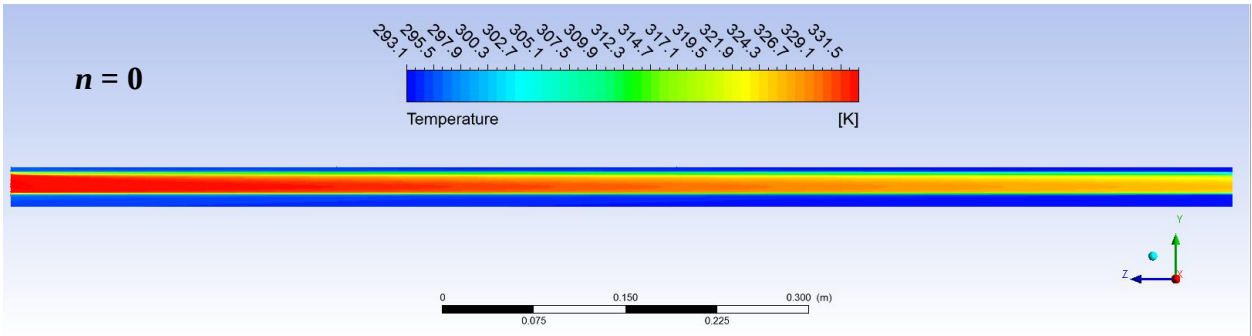

Figure 28 Temperature Contour along Z-Axis Iteration n= 0 Pipe at Re = 10000

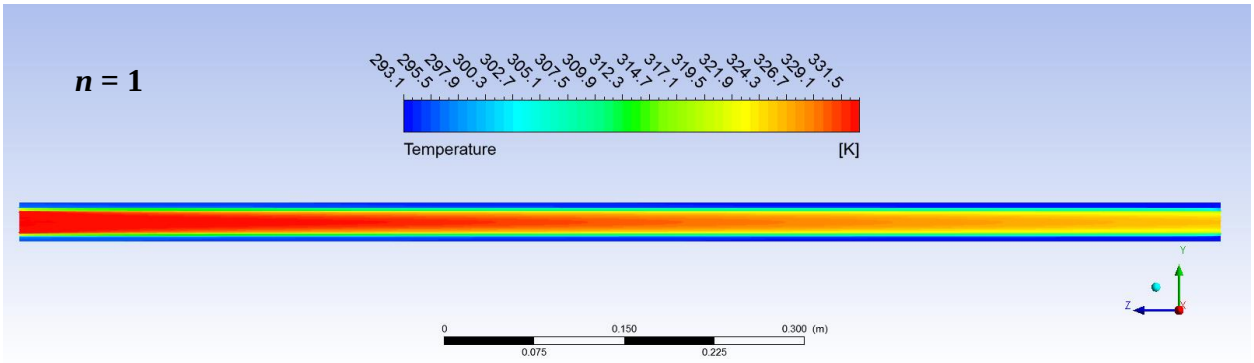

Figure 29 Temperature Contour along Z-Axis Iteration *n* = 1 Pipe at Re = 10000

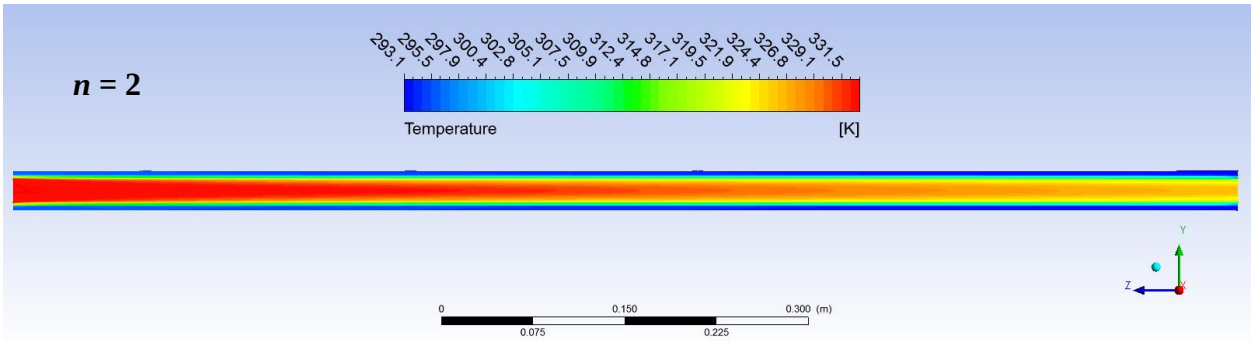

Figure 30 Temperature Contour along Z-Axis Iteration *n* = 2 Pipe at Re = 10000

Re = 25,000

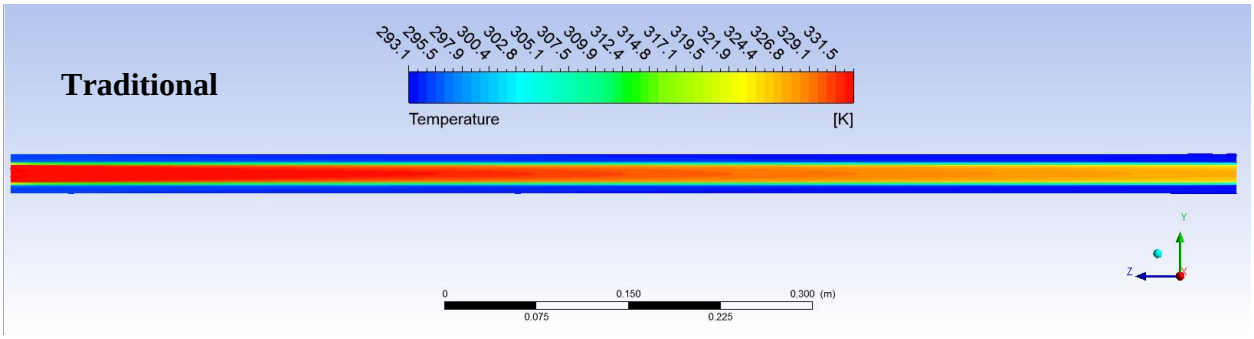

Figure 31 Temperature Contour along Z-Axis Traditional Pipe at Re = 25000

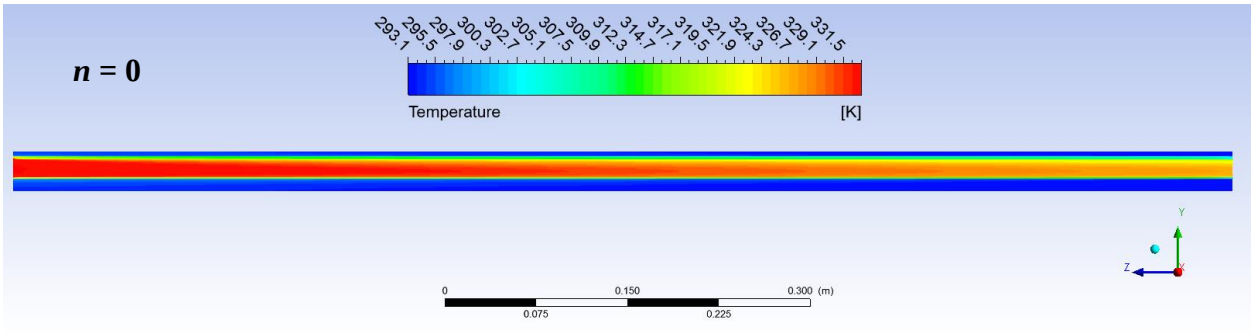

Figure 32 Temperature Contour along Z-Axis Iteration *n* = 0 Pipe at Re = 25000

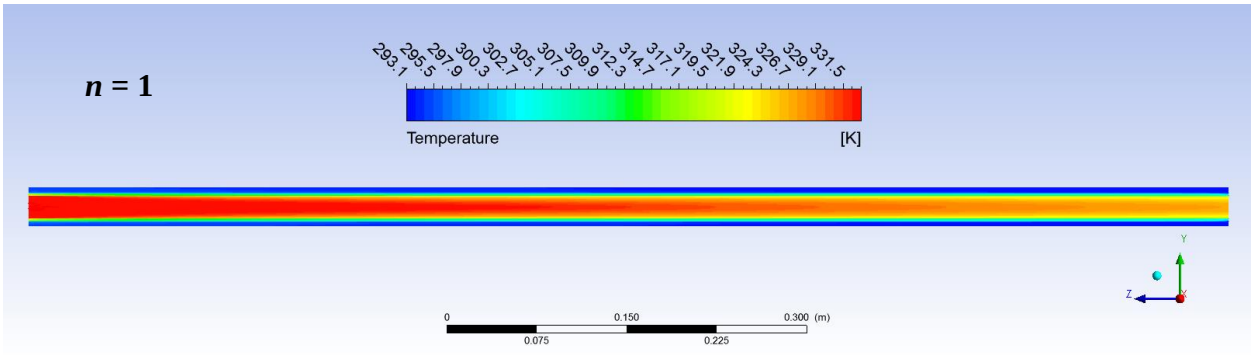

Figure 33 Temperature Contour along Z-Axis Iteration *n* = 1 Pipe at Re = 25000

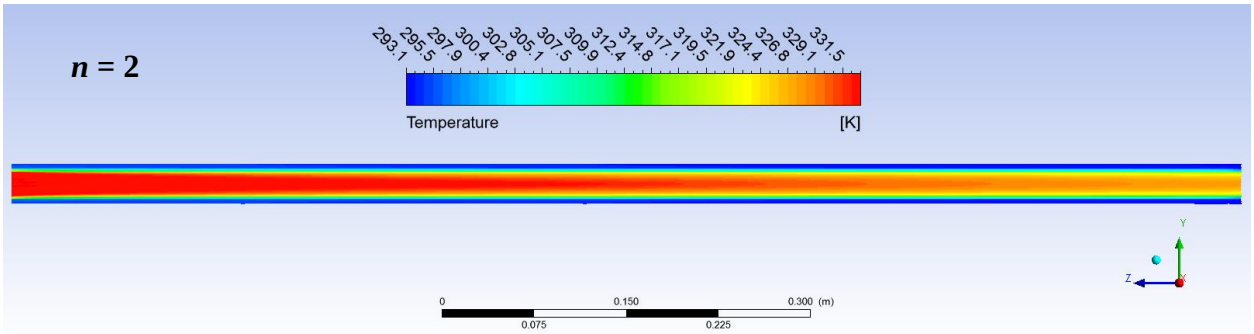

Figure 34 Temperature Contour along Z-Axis Iteration *n* = 2 Pipe at Re = 25000

Re = 40,000

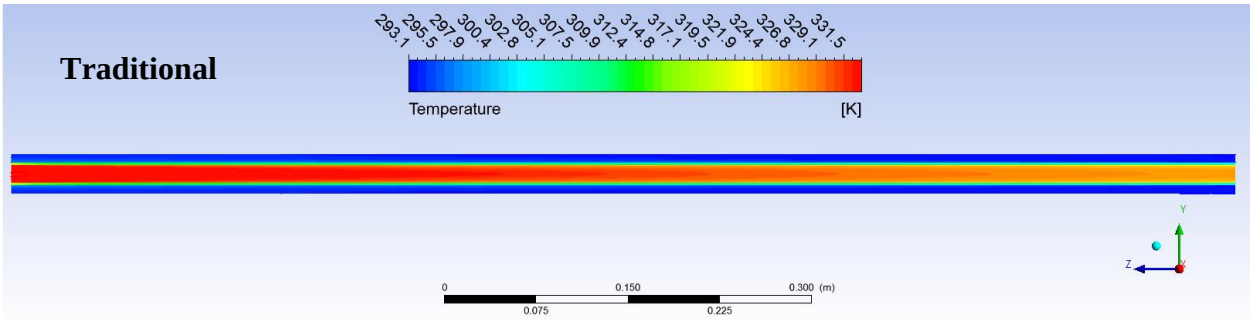

Figure 35 Temperature Contour along Z-Axis Traditional Pipe at Re = 40000

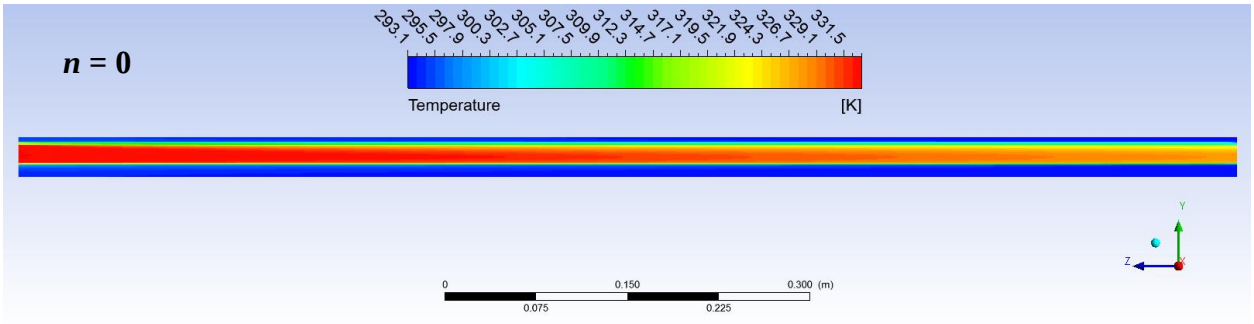

Figure 36 Temperature Contour along Z-Axis Iteration *n* = 0 Pipe at Re = 40000

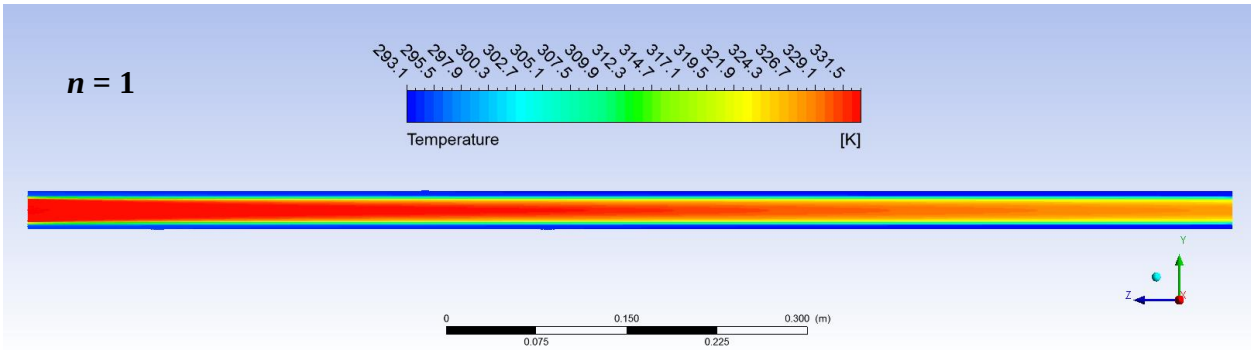

Figure 37 Temperature Contour along Z-Axis Iteration *n* = 1 Pipe at Re = 40000

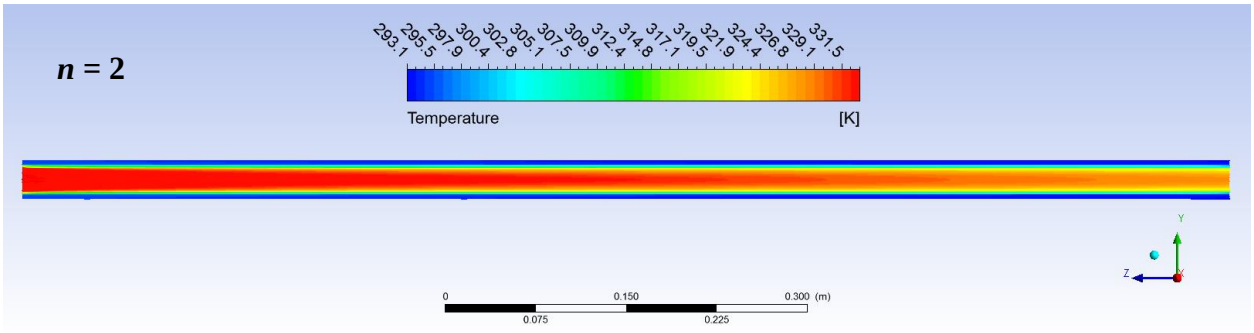

Figure 38 Temperature Contour along Z-Axis Iteration *n* = 2 Pipe at Re = 40000